BEAM SELECTION TECHNIQUES IN MILLIMETER WAVE COMMUNICATIONS

A Thesis Submitted to
the Graduate School of Engineering and Sciences of
İzmir Institute of Technology
in Partial Fulfillment of the Requirements for the Degree of

MASTER OF SCIENCE

in Electronics and Communication Engineering

by
İrem CUMALI

December 2019
İZMİR

ACKNOWLEDGMENTS

ABSTRACT

BEAM SELECTION TECHNIQUES IN MILLIMETER WAVE COMMUNICATIONS

Millimeter wave (mmWave) communication is an advantageous technology which is capable of meeting the needs of future mobile networks. On the other hand, the propagation characteristics and system requirements are the restrictive factors for utilization of mmWave communication. Hybrid and digital beamforming architectures can be evaluated as worthy candidates to utilize mmWave communication. In the hybrid architecture, selection of a few number of beams by exploiting the sparse structure of the beamspace channel provides high spectral efficiency with low complexity.

In this thesis, the multi-user mmWave communication in sparse and dense environments are investigated. Beam selection algorithms presented in the literature are performed for the sparse environment. While the number of users is equal to the number of radio frequency (RF) chains in a sparse environment, the number of RF chains is less than the number of users in a dense environment. Therefore, an algorithm which performs beam and user selection for the dense environment is proposed. The user selection in the proposed beam and user selection algorithm is performed based on the correlation among users' channels. Since the users' channels are highly correlated in mmWave communication, the proposed beam and user selection algorithm improves the spectral efficiency considerably.

Furthermore, a non-uniform rectangular array (NURA) antenna configuration for mmWave communication is investigated when the digital beamforming architecture is employed. Then, a user selection algorithm is proposed under the case of lower number of antennas. The simulation results demonstrate the improvement in sum data rate through the proposed user selection algorithm in mmWave communication with NURA configuration.

ÖZET

MİLİMETRE DALGA HABERLEŞMEDE HÜZME SEÇİM TEKNİKLERİ

Milimetre dalga haberleşmesi, gelecekteki mobil ağların ihtiyaçlarını karşılayabilecek avantajlı bir teknolojidir. Öte yandan, yayılma özellikleri ve sistem gereksinimleri, milimetre dalga haberleşmesinin kullanımını kısıtlayan faktörlerdir. Hibrit ve dijital hüzme oluşturma mimarileri, milimetre dalga haberleşmesini kullanmak için değerli birer aday olarak değerlendirilebilir. Hibrit mimaride, ışın-uzay kanalının seyrek yapısından faydalanarak birkaç hüzmenin seçimi, düşük karmaşıklığa sahip yüksek spektral verimlilik sunmaktadır.

Bu tezde, seyrek ve yoğun ortamlarda çok kullanıcılı milimetre dalga haberleşmesi incelenmektedir. Literatürde sunulan hüzme seçim algoritmaları, seyrek ortam için uygulanmaktadır. Kullanıcı sayısı seyrek bir ortamda radyo frekansı (RF) zincirlerinin sayısına eşit iken, yoğun bir ortamda RF zinciri sayısı kullanıcı sayısından daha azdır. Bu nedenle, yoğun ortamlar için hüzme ve kullanıcı seçimlerini birlikte gerçekleştiren bir algoritma önerilmiştir. Önerilen hüzme ve kullanıcı seçim algoritmasındaki kullanıcı seçimi, kullanıcı kanalları arasındaki korelasyon esas alınarak yapılır. Kullanıcı kanallarının milimetre dalga haberleşmesinde yüksek oranda korelasyon göstermesi nedeniyle, önerilen hüzme ve kullanıcı seçim algoritması spektral verimliliği önemli ölçüde arttırmaktadır.

Ayrıca, dijital hüzme oluşturma mimarisi kullanıldığında, milimetre dalga haberleşmesi için düzenli olmayan dikdörtgen dizi (NURA) anten konfigürasyonları incelenmektedir. Ardından, daha az sayıda anten olması durumunda bir kullanıcı seçim algoritması önerilmektedir. Simülasyon sonuçları, önerilen kullanıcı seçim algoritması yoluyla NURA yapısı ile milimetre dalga haberleşmesindeki toplam veri hızındaki iyileşmeyi göstermektedir.

TABLE OF CONTENTS

LIST OF FIGURES

LIST OF TABLES

LIST OF ABBREVIATIONS

CHAPTER 1

INTRODUCTION

For the next generation mobile networks, various emerging technologies have been defined to respond the need of ever-increasing wireless data traffic. From that viewpoint, millimeter wave (mmWave) communication has drawn great interest over the past few years because of its favourable opportunities. The mmWave spectrum from 30 GHz to 300 GHz has large available bandwidth providing a great enhancement in data rates. Therefore, high data rates can be achieved even with very low spectral efficiency which facilitates the implementation. Moreover, mmWave has small wavelength enabling to fit hundreds of antennas into a small area. Especially for the massive number of antennas, mmWave communication can be the solution of space limitation issue. Another potential of mmWave is the narrow beamwidth causing less interference due to having large number of antenna elements.

On the other hand, there are some challenges about the propagation of mmWave and hardware implementation. The main issue is the high path loss to which the mmWave propagation is exposed. Compared to the microwave frequencies, path loss is higher in mmWave since it has shorter wavelength. This issue restricts the range of communication to a few hundreds of meters (Rappaport et al., 2013). Another challenge about the propagation is the penetration loss related to non-line of sight (NLoS) communication. The signal attenuates highly resulting from the walls and glasses; so the communication between inside and outside become difficult.

For the challenges related to the implementation can be enumerated as high power consumption and hardware complexity. Power consumption is an essential criterion in practice. Because of the high frequency and usage of large number of antennas to compensate the high path loss, the power consuming on the hardware components can be excessive. Furthermore, the complexity of circuitry increases when the large number of antennas are utilized. Therefore, a different approach to beamforming is required to reduce the hardware complexity and power consumption. At that point, hybrid analog/digital beamforming technique can be qualified as the key solution. With this technique, analog and digital beamformers are employed jointly to exploit the benefits of both when the number of antennas are very high. Although the spectral efficiency obtained by using digital beamforming cannot be achieved by hybrid beamforming, it offers the suboptimal

solution with less power requirement.

In a hybrid transmitter, all beams can not be transmitted simultaneously due to the limited number of radio frequency (RF) chains. Hence, the beams to be transmitted are selected depending on a specific criterion, and the selected beams are digitally precoded before the transmission. Herein, the beam selection method plays a decisive role in the system performance. The most spectral efficient beam selection method can be a full search in which all the combinations of beam subsets are investigated. But, this method involves excessive computational load especially for high dimensional array antennas. In the literature, there are many methods identified to avoid such an exhaustive search.

In this thesis, the objective is to design a beam selection algorithm to maximize the sum data rate for dense environments. The methods in the literature address the beam selection issue for sparse environments. While sparse environment contains equal number of users and RF chains, dense environment involves less number of RF chains than that of users. Hence, all users can not be served simultaneously in a dense environment and the system performance can be maximized by utilizing beam and user selection together. In addition, full dimensional multiple-input multiple-output (FD-MIMO) systems for the mmWave communication is investigated. Also, for the non-uniform array antenna structures, the system performance is evaluated.

Throughout the thesis, multi-user mmWave communication systems are investigated in a single cell scenario. The users are randomly located in an outdoor environment and their positions are assumed to be stationary. The thesis is organized as follows:

- In Chapter 2, the propagation characteristics and channel model of the mmWave system are discussed. Beamforming techniques, beamspace system representation and beam selection techniques in literature are examined. Also, the proposed user and beam selection algorithm is presented to maximize the sum data rate and the simulation results for sparse and dense environments are demonstrated.

- Chapter 3 investigates FD-MIMO systems for mmWave communication. For that system, non-uniform rectangular array (NURA) models are examined and a decremental user selection algorithm based on the correlation between the users' channels is proposed to maximize the system sum data rate. The performance comparisons between uniform rectangular array (URA) and NURA and the performance of the proposed user selection algorithm are provided.

- Chapter 4 summarizes the interpretation of the results and gives the future research directions.

CHAPTER 2

BEAM SELECTION ALGORITHMS

This chapter introduces the concept of millimeter wave communication through a downlink system. The channel model, beamspace representation of the system, beamforming techniques that are used in lower frequencies and their applicability to mmWave systems are provided. Moreover, the beam selection techniques in literature and the proposed algorithm are represented for the given system. Eventually, the simulation results are demonstrated for the different environments, the number of antennas, the types of precoders.

2.1. System Model

In this thesis, a downlink communication system which contains a base station (BS) and multiple users is dealt with. At the BS, a discrete lens array (DLA) revealing the concept of beamspace multiple-input multiple-output (MIMO) is utilized. In order to model the DLA, it can be possible to use a uniform linear array (ULA) which is composed of identical antenna elements. The number of antenna elements in the array is denoted by N_{T}. The spacing between each element is described as the half of the carrier wavelength, which corresponds to critically sampled ULA. In addition, a linear precoder is employed at the digital part of the BS, and there are N_{RF} RF chains.

At the receiver side, the total number of users is K in which each with a single antenna. Two different systems depending on the environment are investigated. The system that is called as *sparse system* refers to a system which satisfies $N_{\mathrm{T}} \gg K$ and $N_{\mathrm{RF}} = K$ when N_{T} is sufficiently large. For this system, beam selection algorithm is carried out so that K beams are assigned for K users. On the other hand, *dense system* contains K users which meet $N_{\mathrm{T}} \gg K > N_{\mathrm{RF}}$. However, the BS can serve as many users as the number of RF chains, simultaneously. For this reason, the dense system requires a user selection algorithm in addition to beam selection. Hence, for the dense system, both user and beam selection algorithms are applied. In overall, the BS communicates with several users through millimeter wave propagation in dense or sparse environments.

The received signal for the kth user is given as:

$$r_k = \mathbf{h}_k^H \mathbf{x} + n_k \tag{2.1}$$

where $\mathbf{h}_k \in \mathbb{C}^{N_\mathrm{T} \times 1}$ is the channel vector and $n_k \sim \mathcal{CN}(0, \sigma^2)$ is the additive white Gaussian noise (AWGN) for the kth user, $\mathbf{x} \in \mathbb{C}^{N_\mathrm{T} \times 1}$ is the transmitted signal vector defined by $\mathbf{x} = [x_1, x_2, \ldots, x_{N_\mathrm{T}}]^T$. By gathering the received signals for all the K users, the received signal vector $\mathbf{r} = [r_1, r_2, \ldots, r_K]^T$ reveals the system equation in spatial domain as:

$$\mathbf{r} = \mathbf{H}^H \mathbf{x} + \mathbf{n} \tag{2.2}$$

where $\mathbf{H} = [\mathbf{h}_1, \mathbf{h}_2, \ldots, \mathbf{h}_K] \in \mathbb{C}^{N_\mathrm{T} \times K}$ is the channel matrix specifying the system and $\mathbf{n} \in \mathbb{C}^{K \times 1}$ represents the AWGN vector with $\mathbf{n} \sim \mathcal{CN}(0, \sigma^2 \mathbf{I}_K)$ where $\mathbf{I}_K$ is the $K \times K$ identity matrix.

After the linear precoder at the BS is provided, the system equation is described as follows:

$$\mathbf{r} = \mathbf{H}^H \mathbf{P} \mathbf{s} + \mathbf{n} \tag{2.3}$$

where $\mathbf{P} \in \mathbb{C}^{N_\mathrm{T} \times K}$ is the digital precoding matrix, $\mathbf{s} \in \mathbb{C}^{K \times 1}$ is the symbol vector satisfying that the correlation matrix of $\mathbf{s}$ is $\mathbf{\Lambda}_s = \mathbb{E}[\mathbf{s}\mathbf{s}^H] = \mathbf{I}_K$. In other words, the transmitted symbols for all the K users are independent from each other and they have unit energy. Furthermore, the constraint related to the total transmit power ρ is identified by:

$$\mathbb{E}[\|\mathbf{x}^2\|] = \mathrm{tr}(\mathbf{P}\mathbf{\Lambda}_s\mathbf{P}^H) = \mathrm{tr}(\mathbf{P}\mathbf{P}^H) \leq \rho \tag{2.4}$$

where the transmitted signal $\mathbf{x} = \mathbf{P}\mathbf{s}$ and $\mathrm{tr}(.)$ denotes the trace operation.

2.2. Millimeter Wave Channel Model

In a MIMO system including N_T transmit and N_R receive antennas, the spatial channel is directly related to the array steering vector $\mathbf{a}_\mathrm{T}(\theta_\mathrm{T})$ for the transmitter and the

array response vector $\mathbf{a}_R(\theta_R)$ for the receiver. The phase profile of an antenna array is characterized by its array steering/response vector $\mathbf{a}(\theta)$ as a function of spatial angle or direction θ. In other words, the steering vector for the transmit antenna, $\mathbf{a}_T(\theta_T)$ contains the coefficients of each antenna element to concentrate the beam towards the direction θ_T. Likewise, the response vector for the receive antenna $\mathbf{a}_R(\theta_R)$ depicts the discrete signal from the point source in the direction of θ_R.

When an N_T-element uniform linear array (ULA) is considered, the array steering vector, which is an N_T dimensional column vector, can be described as follows:

$$\mathbf{a}(\theta) = \frac{1}{\sqrt{N_T}} \left[e^{-j2\pi\theta m} \right]_{m \in \mathcal{Z}(N_T)} \tag{2.5}$$

where $\mathcal{Z}(N_T) = \left\{ n - (N_T - 1)/2 : n = 0, 1, \ldots, (N_T - 1) \right\}$ is a set which contains the indices of the antenna elements at the BS and they are symmetrically located around zero. The spatial angle θ is defined by:

$$\theta = \left(\frac{d}{\lambda} \right) \sin(\vartheta), \quad d = \lambda/2 \tag{2.6}$$

where $\vartheta \in [-\pi/2, \pi/2]$ is the physical angle, λ is the wavelength of propagation and d is the antenna spacing which satisfies the critical spacing as mentioned before. Therefore, the spatial angle $\theta = 0.5 \sin(\vartheta)$, and it is an element of the range $[-0.5, 0.5]$.

When a uniform rectangular array (URA) is discussed, the array steering vector $\mathbf{a}(\theta, \phi)$ is related to the Kronecker product of the array steering vectors in azimuth and elevation domains. Here, θ is the azimuth angle and ϕ is the elevation angle.

In the most general case, the channel is time varying and its frequency domain representation is defined by the multipath model (Sayeed, 2002), (Sayeed and Sivanadyan, 2010), (Heath et al., 2016):

$$\mathbf{H}(t, f) = \sum_{p=1}^{N_p} \beta^{(p)} e^{j2\pi\upsilon^{(p)}t} e^{-j2\pi\tau^{(p)}f} \mathbf{a}_R\left(\theta_R^{(p)}, \phi_R^{(p)}\right) \mathbf{a}_T^H\left(\theta_T^{(p)}, \phi_T^{(p)}\right) \tag{2.7}$$

where $\beta^{(p)}$ is the gain with complex value, $\upsilon^{(p)}$ is the Doppler shift, $\tau^{(p)}$ is the delay, $\left(\theta_R^{(p)}, \phi_R^{(p)}\right)$ is the angle of arrival (AoA) pair, $\left(\theta_T^{(p)}, \phi_T^{(p)}\right)$ is the angle of departure (AoD) pair for the pth path.

The channel will be almost time invariant if the Doppler shifts of all the paths are assumed to be adequately small, which corresponds to:

$$v^{(p)} \ll \frac{1}{T_s} \quad , \quad p = 1, \dots, N_p \tag{2.8}$$

where T_s is the symbol duration. Hence, it can be expressed as:

$$\mathbf{H}(f) = \sum_{p=1}^{N_p} \beta^{(p)} e^{-j2\pi\tau^{(p)}f} \mathbf{a}_{\mathrm{R}}\left(\theta_{\mathrm{R}}^{(p)}, \phi_{\mathrm{R}}^{(p)}\right) \mathbf{a}_{\mathrm{T}}^H\left(\theta_{\mathrm{T}}^{(p)}, \phi_{\mathrm{T}}^{(p)}\right) \tag{2.9}$$

Additively, the channel is narrowband due to the fact that the delays of all the paths are far smaller compared to the symbol duration:

$$\tau^{(p)} \ll T_s \quad , \quad p = 1, \dots, N_p \tag{2.10}$$

Therefore, the channel matrix can be obtained by:

$$\mathbf{H} = \sum_{p=1}^{N_p} \beta^{(p)} \mathbf{a}_{\mathrm{R}}\left(\theta_{\mathrm{R}}^{(p)}, \phi_{\mathrm{R}}^{(p)}\right) \mathbf{a}_{\mathrm{T}}^H\left(\theta_{\mathrm{T}}^{(p)}, \phi_{\mathrm{T}}^{(p)}\right) \tag{2.11}$$

Adapting the multipath channel model to the mmWave propagation, it is required to count in the line of sight (LoS) component as well as the non-line of sight (NLoS) components. Considered mmWave system with ULA in BS radiates the power only in the azimuth direction, so the elevation angle ϕ is removed. Also, the system has single antenna in all users so that the array response vector for the receiver is equal to 1. Therefore, Eq.(2.11) is revised, thereby describing the channel vector associated with the kth user:

$$\mathbf{h}_k = \beta_k^{(0)} \mathbf{a}_{\mathrm{T}}\left(\theta_{\mathrm{T},k}^{(0)}\right) + \sum_{p=1}^{N_p} \beta_k^{(p)} \mathbf{a}_{\mathrm{T}}\left(\theta_{\mathrm{T},k}^{(p)}\right) \tag{2.12}$$

where $\beta_k^{(0)}$ and $\theta_{\mathrm{T},k}^{(0)}$ represents the channel gain and the angle of departure of the LoS path for the kth user, respectively. It is assumed that each user receives LoS path $|\beta_k^{(0)}| \neq 0, \forall k$.

2.3. Beamspace System Representation

Millimeter wave introduces a quasi-optical propagation by its nature. Therefore, the propagation of LoS component prevails against NLoS components. Accordingly, mmWave channel exhibits a sparse structure which makes the transformation into beamspace system inevitable.

Beamspace system is a virtual representation of the traditional MIMO channel. In the MIMO architecture, DLA at the transmitter realizes this transformation from spatial domain to beamspace domain via the beamforming matrix.

The beamforming matrix $\mathbf{U} \in \mathbb{C}^{N_{\mathrm{T}} \times N_{\mathrm{T}}}$ whose columns are formed from the array steering vectors is determined by:

$$\mathbf{U} = \left[\mathbf{a}\left(\theta_m = \frac{m}{N_{\mathrm{T}}} \right) \right]_{m \in \mathcal{Z}(N_{\mathrm{T}})} \tag{2.13}$$

where the specified directions θ_m are generated by dividing the whole space into N_{T}, evenly. Thus, the beamforming matrix provides N_{T} orthogonal beams. Furthermore, it is a unitary Discrete Fourier Transform (DFT) matrix satisfying $\mathbf{U}\mathbf{U}^H = \mathbf{U}^H\mathbf{U} = \mathbf{I}$. The beamspace channel vector for the kth user is identified as follows:

$$\mathbf{h}_{b,k} = \mathbf{U}^H \mathbf{h}_k \tag{2.14}$$

By extension, the beamspace channel matrix can be written as:

$$\mathbf{H}_b = \mathbf{U}^H \mathbf{H} \tag{2.15}$$

where $\mathbf{H}_b = [\mathbf{h}_{b,1}, \mathbf{h}_{b,2}, \dots, \mathbf{h}_{b,K}] \in \mathbb{C}^{N_{\mathrm{T}} \times K}$ and $\mathbf{h}_{b,k} \in \mathbb{C}^{N_{\mathrm{T}} \times 1}$, $\forall k = 1, 2, \dots, K$.

Hence, the beamspace system equation, which is an equivalent representation of Eq.(2.3) due to the unitary nature of $\mathbf{U}$, is described by:

$$\mathbf{r} = \mathbf{H}_b^H \mathbf{P}_b \mathbf{s} + \mathbf{n} \qquad (2.16)$$

where $\mathbf{P}_b = \mathbf{U}^H \mathbf{P}$ is the beamspace precoder. It is worth mentioning that the beamspace channel has a sparse nature. Sparsity states that the channel has only a few number of non-zero coefficients. In other words, there are slight number of multipath components, which are recessive against LoS components.

2.4. Beamforming Techniques

The MIMO architectures that are used in sub-6 GHz are investigated in that part of the thesis. Additionally, their practicability to mmWave frequencies is examined. For a system with N_T transmit and N_R receive antennas, the transceiver architectures which are based on the digital, analog and hybrid analog/digital beamforming techniques are discussed.

2.4.1. Digital Beamforming

In the conventional architecture as illustrated in Figure 2.1, each antenna in both the transmitter and receiver is connected to a separate RF chain to transmit the parallel data streams. In the transmitter, all the symbols are passed through the signal processing in baseband which is called digital precoding. Also in the receiver, the signal processing called digital combining is executed in the baseband.
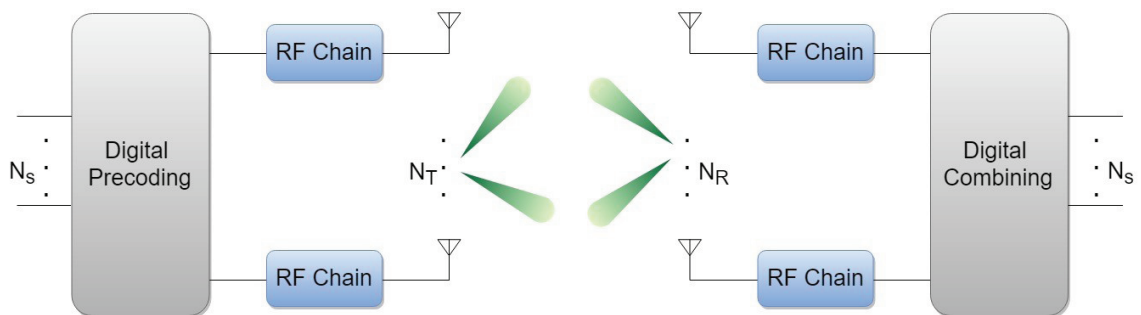
Figure 2.1. MIMO architecture based on digital beamforming.

In mmWave communication, the propagation suffers from high path loss due to the short wavelength of mmWave signals (Shafi et al., 2018). To cope with it by exploiting the array gain, the MIMO architectures come into prominence. Moreover, hundreds of antennas that are critically spaced can be packed into a small area in the mmWave frequencies. However, if the conventional architecture is implemented for a mmWave communication system which employs large number of antennas and has wide bandwidth, it would encounter some problems.

First problem is the implementation and design challenge of the circuitry. Each RF chain involves a low noise amplifier (LNA), power amplifier (PA), digital to analog converter (DAC), analog to digital converter (ADC), RF mixers etc. (Bogale et al., 2016). Therefore, connecting these devices to all the antennas is quite complicated and it needs to occupy large area which is actually limited with the half wavelength.

The second problem is the power consumption of these devices. At high bandwidths as in the case of mmWave, power amplifiers and data converters consume power excessively (Xiao et al., 2017). The power consumption ranges of a single PA, LNA, ADC, voltage controlled oscillator (VCO) and phase shifter in mmWave frequencies are given in (Heath et al., 2016). Therefore, practising fully digital architecture to mmWave would be unreasonable concerning the implementation challenge, space limitation, cost and power consumption. It is required to reduce the number of RF chains so that a low complexity system can be achieved by considering a feasible trade off with the spectral efficiency. That is why, a hybrid analog/digital beamforming which is discussed later is examined and it is more likely to implement.

2.4.1.1. Zero Forcing Precoding

Zero forcing precoding or beamforming is a transmit processing which is designed to ensure that all the users have null interference including inter-symbol and inter-user interferences. The Moore-Penrose inverse of the channel is realized to construct the precoder matrix assuming that the channel is perfectly known at the transmitter.

Considering the system having N_{T} transmit antennas and K single antenna users, the linear precoder matrix can be described as:

$$\mathbf{P} = \alpha \mathbf{F} \tag{2.17}$$

where α is the power scaling factor guaranteeing the condition given in Eq.(2.4) is met.

When $N_\mathrm{T} \gg K$, unscaled precoder matrix is indicated by the following (Joham et al., 2005):

$$\mathbf{F} = \mathbf{H}\big(\mathbf{H}^H\mathbf{H}\big)^{-1} \tag{2.18}$$

where $\mathbf{F} = [\mathbf{f}_1, \mathbf{f}_2, \ldots, \mathbf{f}_K] \in \mathbb{C}^{N_\mathrm{T} \times K}$. The scaling factor is then identified as:

$$\alpha = \sqrt{\frac{\rho}{tr\big(\mathbf{F}\mathbf{\Lambda}_s\mathbf{F}^H\big)}} \tag{2.19}$$

where ρ is the total transmit power.

On the other hand, the unscaled precoder matrix is described by the inverse of the channel when $N_\mathrm{T} = K$ (Peel et al., 2005):

$$\mathbf{F} = \mathbf{H}^{-1} \tag{2.20}$$

2.4.1.2. Matched Filter Precoding

Transmit matched filter which is also known as Maximum Ratio Transmission (MRT) is a linear precoding technique. At the receiver, signal to interference ratio (SIR) is maximized. Therefore, it performs well in a case which contains minimal noise (Colon et al., 2015).

The unscaled precoder matrix which is matched with the channel matrix is described as:

$$\mathbf{F} = \mathbf{H} \tag{2.21}$$

Then, the linear precoder matrix which is obtained by multiplying Eq.(2.21) with Eq.(2.19) is defined by:

$$P = \sqrt{\frac{\rho}{tr\left(\mathbf{H}\mathbf{\Lambda}_s\mathbf{H}^H\right)}}\,\mathbf{H} \tag{2.22}$$

2.4.1.3. QR Precoding

Another linear precoding technique which is presented in (Hegde and Srinivas, 2019) exploits QR decomposition of the channel such that:

$$\mathbf{H}^H = \mathbf{R}^H\mathbf{Q}^H \tag{2.23}$$

where $\mathbf{Q}$ and $\mathbf{R}$ are unitary and upper triangular matrices, respectively. $\mathbf{Q}$ matrix constructs an orthonormal basis by its columns. After the decomposition, the system in Eq.(2.3) is expressed as:

$$\mathbf{r} = \mathbf{R}^H\mathbf{Q}^H\mathbf{P}\mathbf{s} + \mathbf{n} \tag{2.24}$$

Then, the unscaled precoder matrix is identified by:

$$\mathbf{F} = \mathbf{Q}\mathbf{L}^{-1}\mathbf{L}_D \tag{2.25}$$

where $\mathbf{L} = \mathbf{R}^H$ and diagonal matrix $\mathbf{L}_D$ is generated with the diagonal elements of $\mathbf{L}$. When the scaling factor α defined in Eq.(2.19) is used, the system in Eq.(2.24) is then rewritten as:

$$\mathbf{r} = \alpha\mathbf{L}\mathbf{Q}^H\mathbf{Q}\mathbf{L}^{-1}\mathbf{L}_D\mathbf{s} + \mathbf{n} \tag{2.26}$$

Due to the fact that $\mathbf{Q}$ matrix is unitary satisfying $\mathbf{Q}^H\mathbf{Q} = \mathbf{I}_k$, the system equation can be revised as:

$$\mathbf{r} = \alpha\mathbf{L}_D\mathbf{s} + \mathbf{n} \tag{2.27}$$

Therefore, the precoder provides an interference free system since $\mathbf{L}_D$ is a diagonal matrix. However, it can be utilized only for square channel matrices due to the diagonalization and inverse operations.

For all precoders described for the hybrid case, the beamspace precoders can be obtained by applying Eq.(2.18), Eq.(2.21) and QR decomposition in Eq.(2.23) to $\tilde{\mathbf{H}}_b$ which will be described in next sections.

2.4.2. Analog Beamforming

Analog only beamforming is a basic low complexity technique to implement MIMO. Phase shifters, each is connected to a separate antenna element, are commonly used to steer the beams as indicated in Figure 2.2. Furthermore, only one RF chain is connected to the analog circuitry; so the system complexity and hardware cost are considerably diminished compared to fully digital architecture.
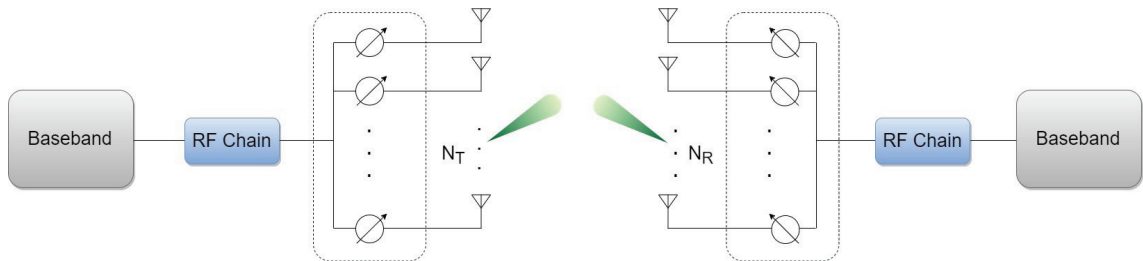
Figure 2.2. MIMO architecture based on analog beamforming.

On the contrary, there are some points restricting the utilization of analog based architecture. Analog only beamforming could not support a multi-stream transmission to obtain the spatial multiplexing gain. Moreover, the phase shifters can only arrange the phase of the signals, not the amplitudes. Hence, tuning the beams properly by arranging the weights of the phase shifters can be a trouble especially when the mobility exists.

2.4.3. Hybrid Analog/Digital Beamforming

Hybrid analog/digital beamforming is a new architecture that combines the advantages of fully digital and analog architectures mentioned before. Actually, it can

be expressed as an analog architecture which can realize the multi-stream transmission with a lower complexity compared to digital beamforming (Alkhateeb et al., 2014). In Figure 2.3, the number of symbols N_s, the number of RF chains in the transmitter L_T and that in the receiver L_R can be related as: $1 < N_\mathrm{s} < L_\mathrm{T} < N_\mathrm{T}$ and $1 < N_\mathrm{s} < L_\mathrm{R} < N_\mathrm{R}$.
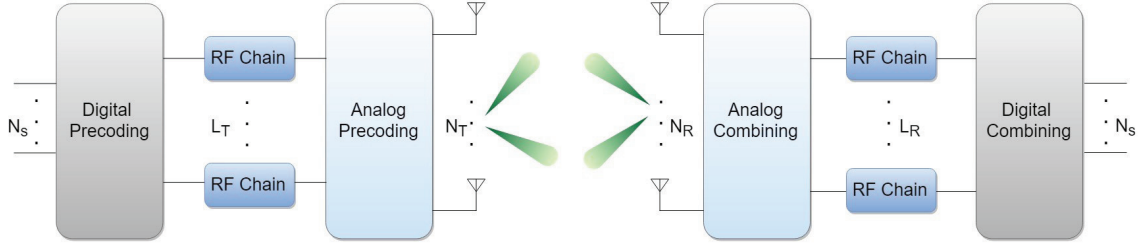
Figure 2.3. MIMO architecture based on hybrid beamforming.

The analog precoding and combining parts in Figure 2.3 can be performed with different structures such as: phase shifters, switches or lenses. For the phase shifter based structures, there are two potential way for implementation. At the first, each RF has a connection to all the antennas. At the second, the antennas are grouped each other and each RF chain is connected to a separate antenna group.

On the other hand, as in the subject of this thesis, a continuous aperture phased (CAP) MIMO architecture based on discrete lens antenna could be used for the analog part of the hybrid transceiver (Brady et al., 2013). This way make available to get much less complicated hardware structure by enabling the beamspace channel accessible. In place of the antennas and analog precoding/combining parts, a beam selection part and lens antenna is employed as demonstrated in Figure 2.4.
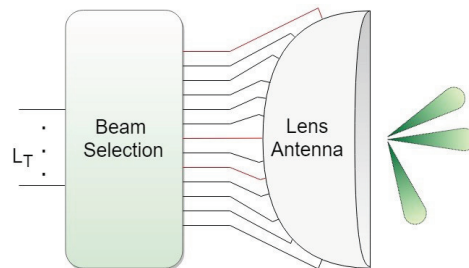
Figure 2.4. CAP-MIMO architecture based on lens antenna.

The lens antenna realizes the beamforming matrix $\mathbf{U}$ as investigated before. Therefore, a great interest in the next stage will be to design the beam selection algorithm and the digital precoding part of the hybrid architecture.

2.5. Beam Selection Techniques

Beam selection makes a low complexity system available by utilizing the sparse nature of the beamspace channel. Thus, not only the hardware complexity and the dimension of the system are reduced but also no significant performance loss occurs. Therefore, by selecting the ith row of the beamspace channel matrix, the reduced dimensional beamspace channel matrix $\tilde{\mathbf{H}}_b$ is constructed:

$$\tilde{\mathbf{H}}_b = \left[\mathbf{H}_b(i,:)\right]_{i \in \mathcal{S}} \tag{2.28}$$

where $\mathcal{S}$ is a set involving the indices of beams which are chosen to be transmitted. Therefore, Eq.(2.16) with lower dimension is given as follows:

$$\mathbf{r} = \tilde{\mathbf{H}}_b^H \tilde{\mathbf{P}}_b \mathbf{s} + \mathbf{n} \tag{2.29}$$

where $\tilde{\mathbf{P}}_b \in \mathbb{C}^{\ell \times K}$ is the reduced dimensional precoder matrix which corresponds to $\tilde{\mathbf{H}}_b \in \mathbb{C}^{\ell \times K}$ and $\ell = |\mathcal{S}|$ where $\ell \leq K$.

For the mmWave MIMO system discussed in this study, several beam selection methods are available in the literature and different selection criteria are handled such as magnitude maximization (Sayeed and Brady, 2013), signal to interference plus noise ratio (SINR) maximization and capacity maximization (Amadori and Masouros, 2015). In addition, an interference aware beam selection (Gao et al., 2016), an iterative beam selection (Pal et al., 2018), an ant colony optimization (ACO) based beam selection (Qiu et al., 2018) and Greedy beam selection (Pal et al., 2019) algorithms have been presented in the literature.

2.5.1. Maximum Magnitude Beam Selection

A beam selection algorithm which is referred as maximum magnitude (MM) beam selection is presented in (Sayeed and Brady, 2013). The paper investigates the effects of using three different reduced dimensional beamspace precoders such as Zero Forcing (ZF), Matched Filter (MF) and Wiener Filter (WF) on overall system capacity. In the simplest manner, MM algorithm used in that investigation is selecting a beam/beams whose magnitude is bigger than the other possible beams for that user. In this regard, channel or sparsity masks for each user is defined to indicate the dominant beams :

$$\mathcal{M}_k = \left\{ m \in \mathcal{Z}(N_{\mathrm{T}}) : |h_{b,k}(m)|^2 \geq \gamma_k \max_m |h_{b,k}(m)|^2 \right\} \tag{2.30}$$

where γ_k is the threshold taking a value between 0 and 1. Then, the mask for all the users can be denoted as:

$$\mathcal{M} = \bigcup_{k=1,\ldots,K} \mathcal{M}_k \tag{2.31}$$

where $\ell = |\mathcal{M}|$ is the total number of beams to be selected. It should be noted that ℓ varies depending on the channel.

If the mask is for selecting d strongest beam for each user, it is called d-beam mask. The algorithm aims to transmit d strongest beam so that each user receives the maximum power. To ensure that, threshold γ_k is individually determined for all the K users.

(Sayeed and Brady, 2013) assumes that NLoS components for all the users have zero path gains, meaning that the channel is strictly LoS. However, the channel model with multipath components would be more realistic and the performance of the algorithm in such an environment should be investigated as well. Furthermore, MM algorithm neglects the multi-user interference which considerably restricts the system performance. When the users are nearly located, the channel will be highly correlated as in mmWave propagation. Therefore, the sparsity mask assigns the same beam for the users whose channels are similar. It is presented in (Gao et al., 2016) that the probability of assigning the same dominant beam to more than one user is extremely high especially when the large number of antennas exists at the BS. Hence, the users are exposed to a serious

multi-user interference. On the other hand, assigning the same beam results in a mis-use of RF chains. According to the channel condition, the number of active RF chains in the system is altered, which is undesirable.

2.5.2. Maximization of SINR Beam Selection

This beam selection algorithm is given in (Amadori and Masouros, 2015). The criterion is SINR, which the algorithm aims to maximize. In order to derive the SINR, the precoder must be described. The low-complexity linear precoder matrix in Eq.(2.17) is used. Therefore, the received SINR for the kth user is analytically expressed as:

$$\text{SINR}_k(\rho) = \frac{\frac{\rho|\alpha|^2}{K}\left|\mathbf{h}_k^H\mathbf{f}_k\right|^2}{\frac{\rho|\alpha|^2}{K}\sum_{i\neq k}\left|\mathbf{h}_i^H\mathbf{f}_k\right|^2 + \sigma^2} \tag{2.32}$$

where α is the scaling factor defined in Eq.(2.19) and σ^2 is the noise power. The ZF precoder eliminates the interference term in Eq.(2.32) which is stated by the summation and provides the received power as $\frac{\rho|\alpha|^2}{K}$. Thus, the SINR can be rewritten as:

$$\text{SINR}_k = \frac{\rho|\alpha|^2}{K\sigma^2} \tag{2.33}$$

where the total transmit power is equally shared among the users.

The algorithm aims to disabled a beam whose elimination maximizes the SINR of the remaining system. In Eq.(2.33), only α is subject to the channel, so the criterion to maximize the SINR can be degraded to:

$$\delta = \arg\max_j\left(\text{SINR}^{(j)}\right) = \arg\max_j\left(\left|\alpha^{(j)}\right|^2\right) \tag{2.34}$$

where $\alpha^{(j)}$ corresponds to $\mathbf{H}^{(j)}$ which is the remaining channel matrix after j^{th} beam is disabled, and δ is the index of the disabled beam.

2.5.3. Interference Aware Beam Selection

The interference aware (IA) beam selection is suggested in (Gao et al., 2016). The algorithm purposes to solve the multi-user interference problem that comes to exist in MM algorithm. For that purpose, the algorithm is accomplished in two stages.

First stage is to classify the users as interference users and non-interference users which are denoted as IUs and NIUs, respectively. The index of dominant beams ε_k for each user is specified, at first. The set of dominant beam index is described as:

$$\mathcal{D} = \left\{ \varepsilon_k \mid k \in \{1, \ldots, K\}, \ \varepsilon_k \in \{1, \ldots, N_\mathrm{T}\} \right\} \tag{2.35}$$

Then, the kth user is assigned as IU if the dominant beam of the kth user is the same as the dominant beam of another user/users. Otherwise, it is assigned as NIU for which the set of user index is $\mathcal{S}_{NIU} = \{1, \ldots, K\} - \mathcal{S}_{IU}$ where $\mathcal{S}_{IU}$ represents the set of user index for IUs. The assigned beams for NIUs is defined by $\mathcal{D}_{NIU} = \left\{ \varepsilon_i \mid i \in \mathcal{S}_{NIU} \right\}$.

At the second stage, the algorithm investigates the beams for IUs to maximize the sum rate. A beam is added to the set of selected beams in each iteration.

2.5.4. Iterative Beam Selection

(Pal et al., 2018) gives both an algorithm for selecting the beams iteratively and an algorithm for generating a precoder which offers to remove the multi-user interference entirely. In each iteration, the beam selection algorithm omits the beam whose absence causes the minimal loss in the sum rate. In total, $N_\mathrm{T} - K$ beams are omitted, which corresponds to selecting K beams for K users.

The process begins with the QR decomposition of the reduced dimensional channel matrix $\tilde{\mathbf{H}}_b$ which is shown below:

$$\tilde{\mathbf{H}}_b = \tilde{\mathbf{Q}}\tilde{\mathbf{R}} \tag{2.36}$$

where $\tilde{\mathbf{Q}}$ is a $K \times K$ orthogonal matrix which is also unitary and $\tilde{\mathbf{R}}$ is a $K \times K$ upper triangular matrix.

When $\tilde{\mathbf{P}}_b = \tilde{\mathbf{Q}}$, the system equation in Eq.(2.29) will be in the following:

$$\mathbf{r} = \left(\tilde{\mathbf{Q}}\tilde{\mathbf{R}}\right)^H \tilde{\mathbf{Q}}\mathbf{s} + \mathbf{n} = \tilde{\mathbf{R}}^H\mathbf{s} + \mathbf{n} \qquad (2.37)$$

Since $\tilde{\mathbf{R}}^H$ is the lower triangular matrix, the received signal for the kth user contains the interference signal resulting from the ith user where $i < k$. Therefore, $\tilde{\mathbf{R}}^H$ should be a diagonal matrix so that no user can interfere each other. For that purpose, the precoder matrix is described by $\tilde{\mathbf{P}} = \tilde{\mathbf{Q}}\mathbf{G}$ where $\mathbf{G}$ is a square matrix, and the received signal is:

$$\mathbf{r} = \tilde{\mathbf{R}}^H\mathbf{G}\mathbf{s} + \mathbf{n} \qquad (2.38)$$

The algorithm for generating the precoder matrix investigates $\mathbf{G}$ matrix that makes $\tilde{\mathbf{R}}^H\mathbf{G}$ diagonal. The other algorithm aims to determine $\tilde{\mathbf{H}}_b$ matrix as mentioned.

2.5.5. Greedy Beam Selection

Greedy beam selection algorithm is presented in (Pal et al., 2019). The algorithm selects beams iteratively and every user is necessarily served. For the beamspace channel, a gain matrix is constructed by:

$$\mathbf{M}(k, n) = \left|\mathbf{H}_b^H(k, n)\right|^2 \qquad (2.39)$$

where $k = 1, \ldots, K$ and $n = 1, \ldots, N_{\mathrm{T}}$. Then, the algorithm determines the strongest beams for each user like in the sparsity masks in Eq.(2.30). For the users sharing the same strongest beam, their shared beam is allocated to the user that has higher channel gain. For example, for both the ith and j^{th} users, the strongest beam is the mth beam. Then, if $\mathbf{M}(i, m) > \mathbf{M}(j, m)$, m^{th} beam is allocated to i^{th} user otherwise it is allocated to j^{th} user. In each iteration, allocated beams and users are deleted from their sets. If the set of unallocated users has some elements, the algorithm will continue. Thus, each user is served by an unshared beam.

2.5.6. Proposed User and Beam Selection Algorithm

In this thesis, two different environments including sparse and dense are investigated. For the sparse environment, Figure 2.5 represents the system which is includes equal number of users and RF chains. For this system, the relation between the number of BS antennas, the number of RF chains and the number of users is: $N_\mathrm{T} \gg N_\mathrm{RF} = K$. The algorithms presented in the literature aim to serve all the K users, simultaneously.
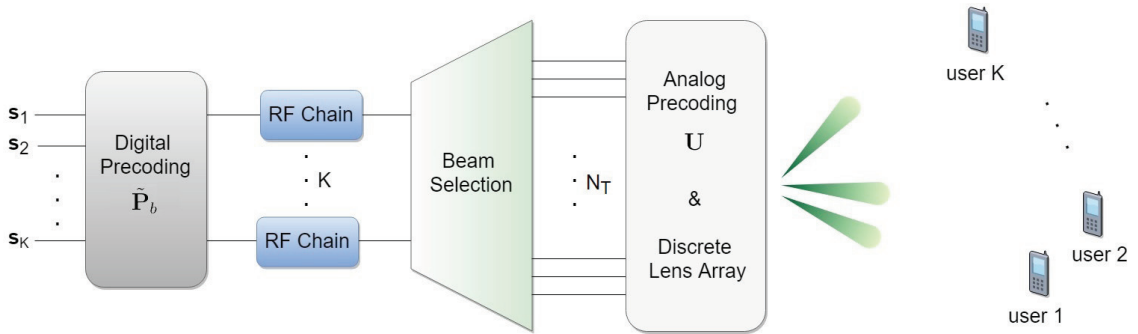
Figure 2.5. Transceiver architecture for the sparse environment.

On the other side, the dense environment contains more users than the number of RF chains and the maximum number of users that can be served is N_RF. Thus, a user selection (US) algorithm is required to select N_RF users among K users. For the proposed system given in Figure 2.6, it is required to apply both user and beam selection processes.
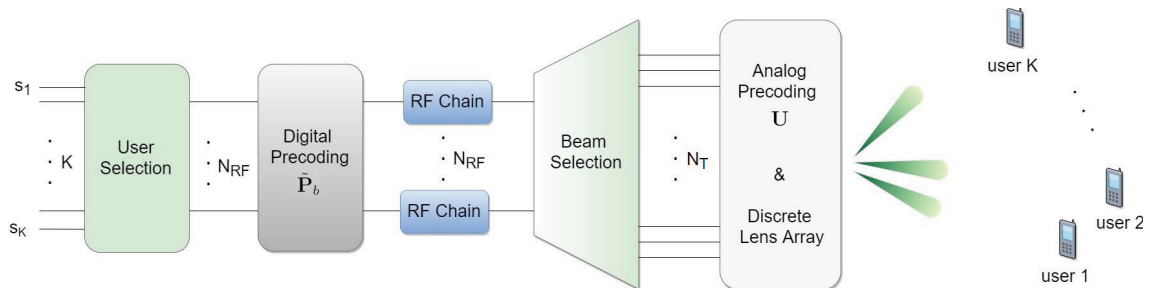
Figure 2.6. Transceiver architecture of the proposed system for the dense environment.

For that purpose, this study presents the low complexity user selection and beam selection algorithms (Cumalı, Özbek, and Pyattaev, 2020) by taking into account highly

correlated user channels, that is inherent in mmWave communication. The flowchart of the proposed user and beam selection algorithm is provided in Figure 2.7.

Firstly, a correlation based user selection algorithm is performed. Most correlated users are eliminated to mitigate the inter-user interference. Therefore, the correlation between i^{th} and j^{th} user is calculated by:

$$c(i, j) = \frac{|\mathbf{h}_{b,i}^{H}\mathbf{h}_{b,j}|}{\|\mathbf{h}_{b,i}\|\|\mathbf{h}_{b,j}\|} \tag{2.40}$$

where $c(i, j)$ takes a real value between 0 and 1 for $i = 1, \ldots, K$ and $j = 1, \ldots, K$ while $i \neq j$. A high correlation value refers to nearly located users due to the predominance of LoS components in mmWave propagation. Therefore, theThen the user pairs that has the correlation greater than the specified threshold c_{th} are determined, namely the users i and j is determined such that:

$$c(i, j) > c_{th} \tag{2.41}$$

Among that user pairs, the user that has the lower channel gain is eliminated, namely $\mathbf{h}_{b,i}$ is removed from $\mathbf{H}_b$ matrix such that:

$$\|\mathbf{h}_{b,i}\| < \|\mathbf{h}_{b,j}\| \tag{2.42}$$

In this manner, the algorithm can select different number of users depending on the threshold and the channel condition. If the set of selected users are denoted by $\mathcal{U}$, the resulting beamspace channel matrix $\hat{\mathbf{H}}_b$, which is less correlated, can be expressed by selecting the jth column of $\mathbf{H}_b$:

$$\hat{\mathbf{H}}_b = \left[\mathbf{H}_b(:, j)\right]_{j \in \mathcal{U}} \tag{2.43}$$

where $\hat{\mathbf{H}}_b \in \mathbb{C}^{N_{\mathrm{T}} \times p}$ and $p = |\mathcal{U}|$ is the total number of selected users where $p > N_{\mathrm{RF}}$.

After the user selection is performed, beam selection can be applied to serve the selected users with their first or second strongest beams. For the dense environment, Eq.(2.28) needs to be revised as follows:

$$\tilde{\mathbf{H}}_b = \left[\hat{\mathbf{H}}_b(i,:)\right]_{i \in \mathcal{S}} \tag{2.44}$$

where $\ell = |\mathcal{S}|$ and i^{th} row of $\hat{\mathbf{H}}_b$ is selected. Thus, the resulting channel matrix $\tilde{\mathbf{H}}_b$ and the corresponding precoder matrix $\tilde{\mathbf{P}}_b$ have the dimension of $\ell \times N_{\mathrm{RF}}$ where $\ell = N_{\mathrm{RF}} \leq K$.

For the beam selection, the most dominant beam (or the 1st strongest beam) is determined for each selected users initially. This corresponds to finding 1-beam sparsity masks $\mathcal{M}_1, \mathcal{M}_2, \ldots, \mathcal{M}_p$ as in MM algorithm where $\mathcal{M}_p$ denotes the set containing the strongest beam for the pth user. Then, the 2nd strongest beams are also specified for each selected users.

At that point, the algorithm controls whether the most dominant beams of two or more users coincide or not. If they do not, the algorithm assigns their most dominant beams for each selected user. In this case, there will be no problem associated with the multi-user interference. But if they coincide, which is likely to occur in the proposed system, the algorithm has to take the interference into consideration. Hence, just like in the IA selection algorithm, the users are classified as interference users (IUs) and non-interference users (NIUs), and the set of user index for NIUs and IUs are denoted by $\mathcal{S}_{NIU}$ and $\mathcal{S}_{IU}$, respectively.

If the number of NIUs, $|\mathcal{S}_{NIU}|$ is greater than N_{RF}, the algorithm has to select N_{RF} users and the corresponding most dominant beams. In order to do that, channel gains of NIUs are considered, namely the users that have higher channel gains are selected until the total number of users to be served reaches N_{RF}. The selected users in NIUs are served by their most dominant beams. Therefore, that beams are selected and added to the set $\mathcal{S}$. On the other hand, if $|\mathcal{S}_{NIU}|$ is less than N_{RF}, it is required to add $N_{\mathrm{RF}} - |\mathcal{S}_{NIU}|$ users among IUs. Due to the fact that an IU shares the same strongest beams with another IUs, the algorithm must search the primarily selectable users among IUs. For that purpose, the users having the same 1st strongest beams, called as *beam partners* are found out. In other words, the set $\mathcal{S}_{IU}$ is separated to its subsets and each of the subsets is formed by beam partners. For each subset, the algorithm chooses one user whose 1st beamspace channel gain is the greatest one among its 1st beam partners. These users construct the set $\mathcal{S}_{IU_1}$ and these users will be served by their 1st strongest beams.

Then, the algorithm controls whether $|\mathcal{S}_{IU_1}|$ is sufficient or not. If it is higher than $N_{\mathrm{RF}} - |\mathcal{S}_{NIU}|$, the algorithm chooses $N_{\mathrm{RF}} - |\mathcal{S}_{NIU}|$ users having higher channel gains among $\mathcal{S}_{IU_1}$. Also, their most dominant beams are selected and added to the set $\mathcal{S}$. If it is not sufficient, adding $N_{\mathrm{RF}} - (|\mathcal{S}_{NIU}| + |\mathcal{S}_{IU_1}|)$ users from the set of remaining users $\mathcal{S}_{IU_2}$ satisfying $\mathcal{S}_{IU_2} = \mathcal{S}_{IU} \setminus \mathcal{S}_{IU_1}$ is needed. If $|\mathcal{S}_{IU_2}|$ is higher than the required number of
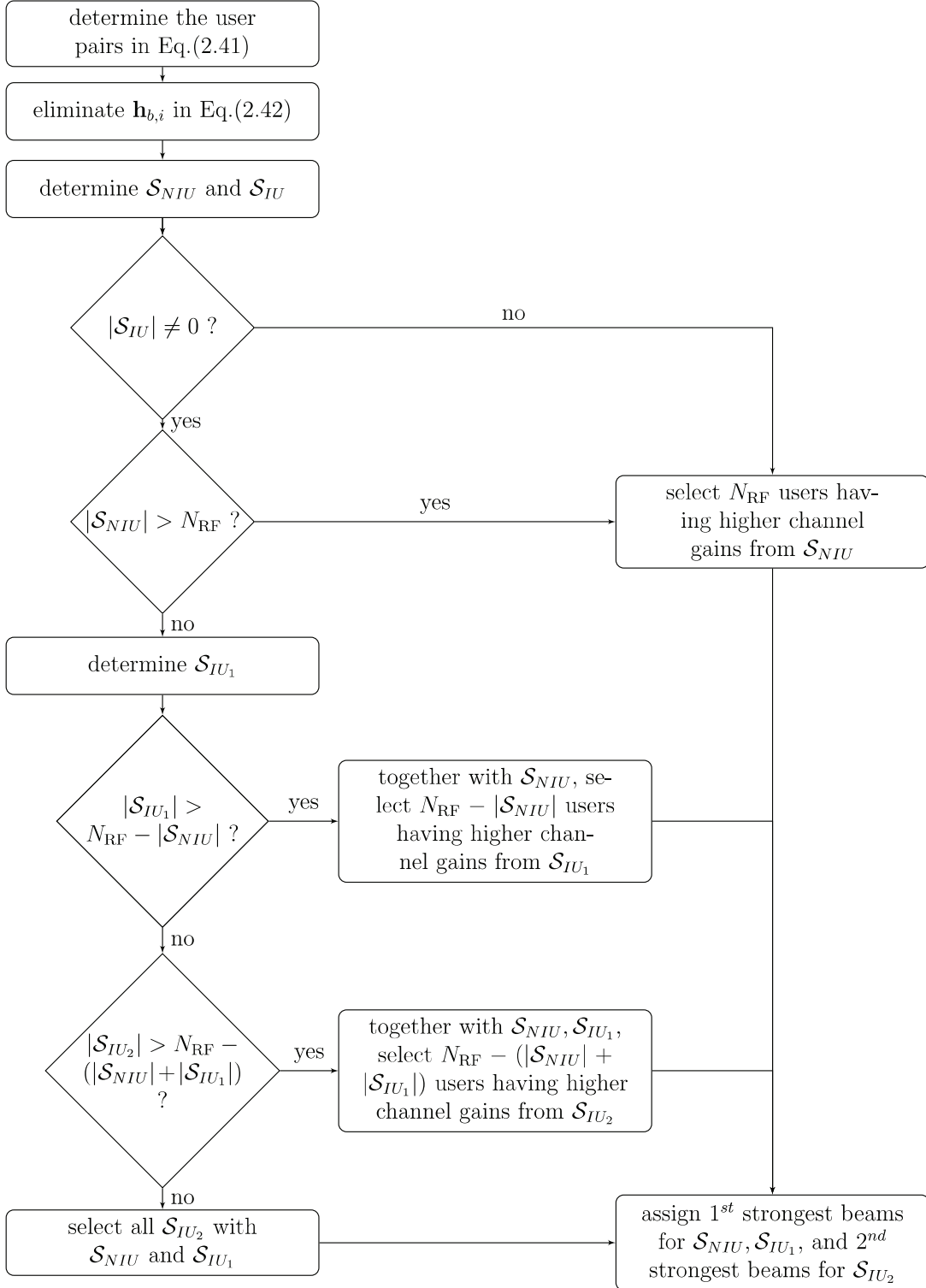
determine the user pairs in Eq.(2.41)

eliminate $\mathbf{h}_{b,i}$ in Eq.(2.42)

determine $\mathcal{S}_{NIU}$ and $\mathcal{S}_{IU}$

$|\mathcal{S}_{IU}| \neq 0$?

no

yes

$|\mathcal{S}_{NIU}| > N_{\text{RF}}$?

yes

select N_{RF} users having higher channel gains from $\mathcal{S}_{NIU}$

no

determine $\mathcal{S}_{IU_1}$

$|\mathcal{S}_{IU_1}| > N_{\text{RF}} - |\mathcal{S}_{NIU}|$?

yes

together with $\mathcal{S}_{NIU}$, select $N_{\text{RF}} - |\mathcal{S}_{NIU}|$ users having higher channel gains from $\mathcal{S}_{IU_1}$

no

$|\mathcal{S}_{IU_2}| > N_{\text{RF}} - (|\mathcal{S}_{NIU}| + |\mathcal{S}_{IU_1}|)$?

yes

together with $\mathcal{S}_{NIU}, \mathcal{S}_{IU_1}$, select $N_{\text{RF}} - (|\mathcal{S}_{NIU}| + |\mathcal{S}_{IU_1}|)$ users having higher channel gains from $\mathcal{S}_{IU_2}$

no

select all $\mathcal{S}_{IU_2}$ with $\mathcal{S}_{NIU}$ and $\mathcal{S}_{IU_1}$

assign 1st strongest beams for $\mathcal{S}_{NIU}, \mathcal{S}_{IU_1}$, and 2nd strongest beams for $\mathcal{S}_{IU_2}$

Figure 2.7. Flowchart of the proposed user and beam selection algorithm.

users, the users having higher channel gains among $\mathcal{S}_{IU_2}$ is selected and their 2nd strongest beams are assigned to these users. Totally, the algorithm selects N_{RF} beams out of N_{T} beams in order to serve N_{RF} users while $K - N_{\mathrm{RF}}$ users are out of service because of the high density of the environment.

2.6. Performance Evaluations

In the simulation environment, we consider a downlink mmWave communication system with N_{T} transmit antennas and N_{RF} RF chains, communicating with K single-antenna users.

For a system with $N_{\mathrm{T}} = 81$ transmit antennas and $K = N_{RF} = 20$ users, contour plot and 2-beam channel sparsity masks $\mathcal{M}_k$ for all users are demonstrated in Figure 2.8(a) and Figure 2.8(b), respectively. This system assumes that there is only LoS link between BS and each user which are uniformly distributed over the space between (-90, +90) degrees. Furthermore, channel of each user has a unity gain such that $|\beta_k^{(0)}| = 1$, $\forall k$.

For this system, Figure 2.8(a) indicates that the beamspace channel has a sparse nature by demonstrating the beam directions for each user. On the other hand, the first and second strongest beams for each user is indicated with the black boxes in Figure 2.8(b). For example, 59th and 60th beams are the strongest beams for the 1st user. As can be seen in this figure, the first and second strongest beams are always the adjacent beams for all the users. Because this system considers only the LoS propagation. Furthermore, there are many users that share the same strongest beam/beams with the other users. Due to this situation, high inter-user interference occurs as mentioned before.

Apart from the system with pure LoS channels, the performance evaluations in Section 2.6.1 and 2.6.2 are performed for a channel with LoS and NLoS components. For different number of antennas and users, the sum data rate comparisons of three beamspace precoders are provided. For the kth user, the channel vector $\mathbf{h}_k$ which is specified in Eq.(2.12) has the parameters given in the following:

- one LoS path with $\beta_k^{(0)} \sim \mathcal{CN}(0, 1)$,
- two NLoS path with $\beta_k^{(p)} \sim \mathcal{CN}(0, 0.1)$ when $p = 1, 2$.
- one spatial angle for LoS path $\theta_{\mathrm{T},k}^{(0)} \sim \mathcal{U}(-0.5, 0.5)$,
- two spatial angles for NLoS paths $\theta_{\mathrm{T},k}^{(p)} \sim \mathcal{U}(-0.5, 0.5)$ when $p = 1, 2$.
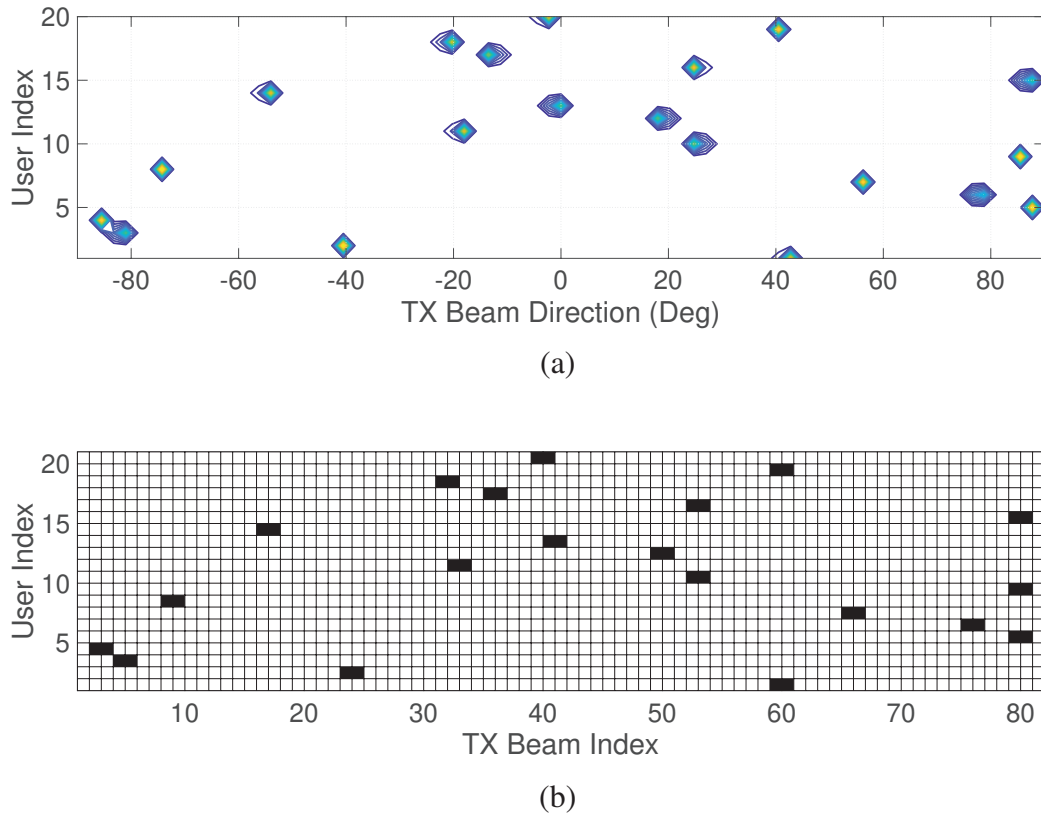
(a)

(b)

Figure 2.8. Demonstrations for the system containing only LoS link: (a) contour plot of $|\mathbf{H}_b^H(k,n)|^2$ for $k = 1, \ldots, K$ and $n = 1, \ldots, N_\mathrm{T}$, (b) 2-beam channel sparsity mask.

2.6.1. Simulation Results in Sparse Environment

In this section, the performance evaluations for the sparse environment are given. In Figure 2.9, the sum data rate results of MM algorithm under the use of MF and ZF precoding are demonstrated for the sparse environment. For the SNR values higher than 21 dB, ZF precoder provides better performance than MF precoder since ZF completely eliminates the interference. MF precoder is interference limited, so this precoding can not manage multi-user interference. For low SNRs, it can reduce the interference due to the asymptotic orthogonality of user channels for sufficiently large number of antennas.

In Figure 2.10, the sum data rate comparison of Greedy algorithm which is described in Section 2.5.5 is demonstrated for the sparse environment. For the SNR values lower than 18 dB, MF precoder outperforms ZF precoder while ZF gives better sum data rate for higher SNR values.
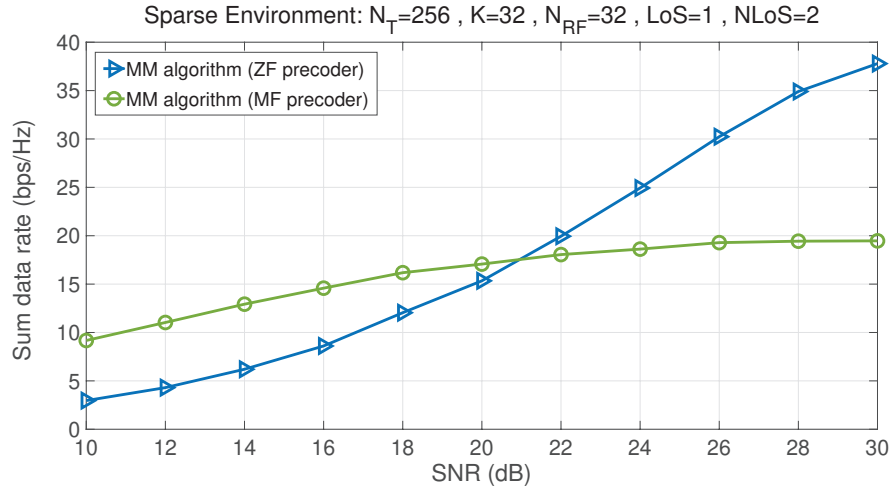
Figure 2.9. Sum data rate results of different precoders for MM algorithm with 256 antennas, 32 users, 32 RF chains and 2 NLoS components.
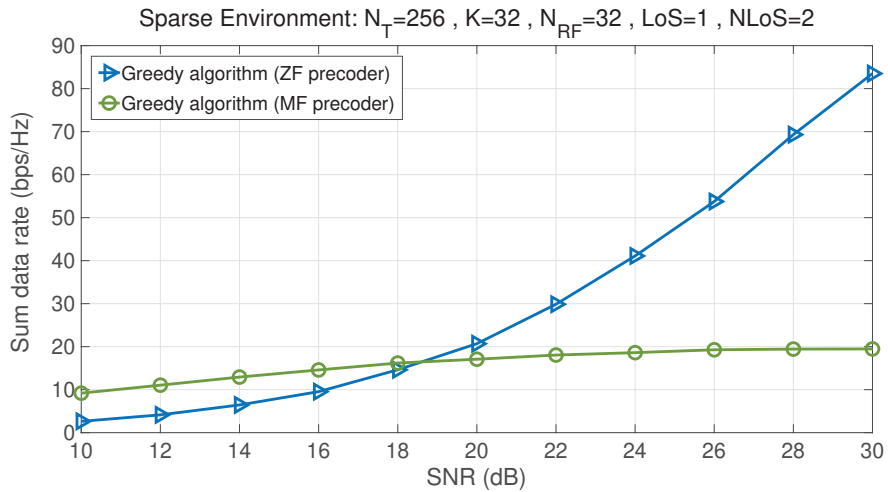

Figure 2.10. Sum data rate results of different precoders for Greedy algorithm with 256 antennas, 32 users, 32 RF chains and 2 NLoS components.

In Figure 2.11, the performance of MM and Greedy algorithms are compared when the ZF precoder is utilized. Greedy algorithm provides much better performance than MM algorithm. Because, Greedy algorithm allocates an unshared beam for each user while MM algorithm can not serve all the users.

In Figure 2.12, the performances of MM and Greedy algorithms for ZF precoder with different number of users are compared. For both algorithms, the sum data rate is decreased when the number of users is increased. Because, as the number of users approaches to the number of antennas, the probability of sharing the same strongest beam

among users is increased. On the other side, ZF precoder degrades the performance while eliminating the interference.
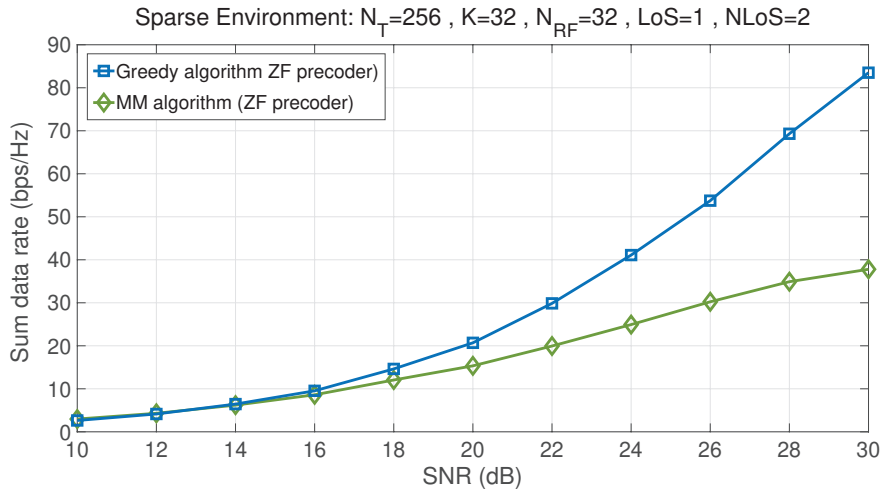

Figure 2.11. Sum data rate results of different algorithms for ZF precoder with 256 antennas, 32 users, 32 RF chains and 2 NLoS components.
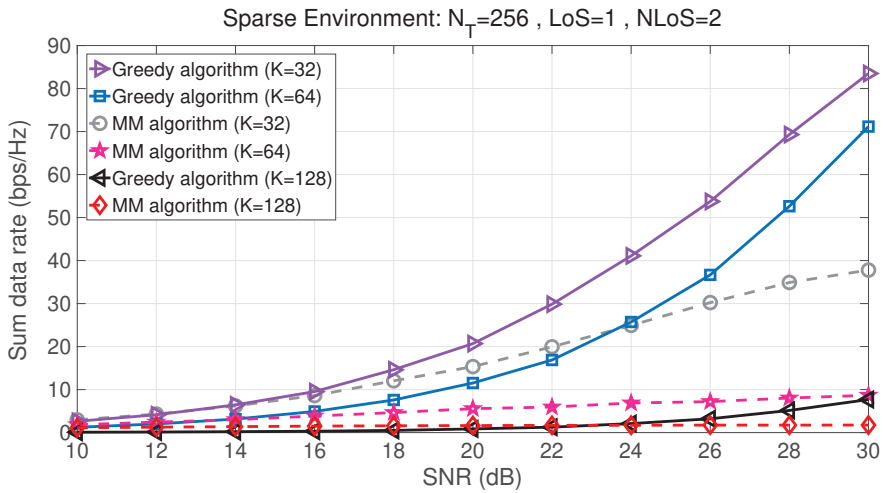

Figure 2.12. Sum data rate results of different number of users for ZF precoder with 256 antennas and 2 NLoS components.

In Figure 2.13, the effect of the number of antennas is provided for ZF precoder while the number of users is kept the same. It is remarkable that the sum data rate is improved by using larger number of antennas for both algorithms. In this way, the probability that some beam partners exist is reduced as mentioned before.
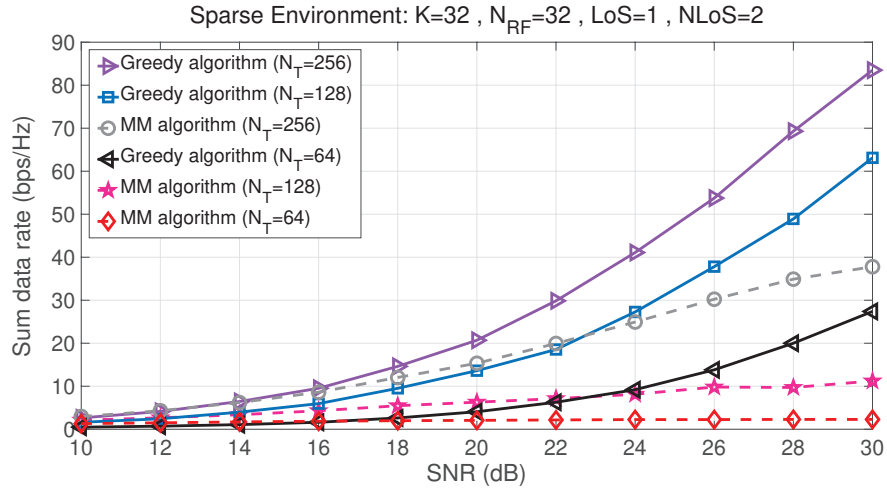
Figure 2.13. Sum data rate results of different number of antennas for ZF precoder with 32 users, 32 RF chains and 2 NLoS components.

2.6.2. Simulation Results in Dense Environment

For the dense environment, performances of the proposed algorithm and MM algorithm are investigated for different number of antennas, users, RF chains, threshold values and types of precoder.

In Figure 2.14, the sum data rate results of MM algorithm is demonstrated for ZF, MF and QR precoders. The best performance is given by the QR precoder for all SNR
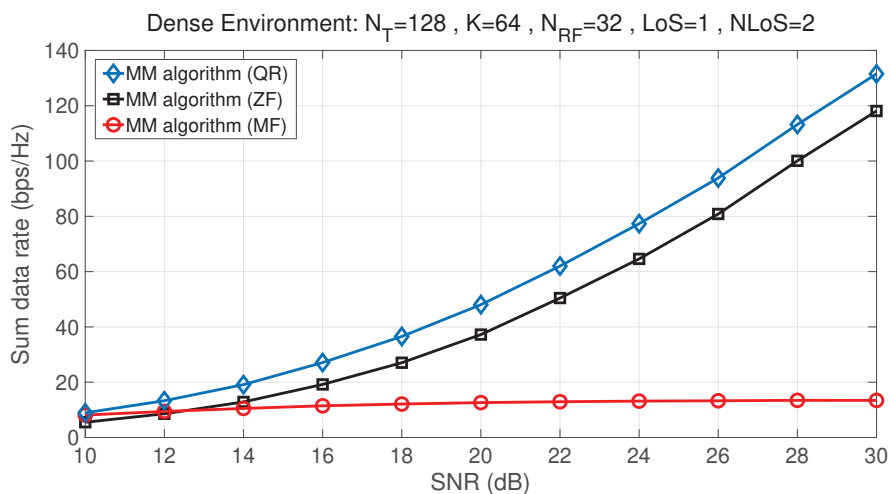

Figure 2.14. Sum data rate results of different precoders for MM algorithm with 128 antennas, 64 users, 32 RF chains and 2 NLoS components.

values. Because it can cancel the interference without degrading the performance unlike ZF. On the other hand, the performance of MF precoder does not give good performance for the increasing SNR values meaning that the residual interference restricts its performance.

In Figure 2.15, the performance of the proposed algorithm for the specified precoders is evaluated when the correlation threshold is 0.2. According to the results, MF precoder provides the worst performance for all SNR values. Also, it is nearly constant over the SNR values. On the other hand, QR precoder provides the highest sum data rates for the proposed algorithm.
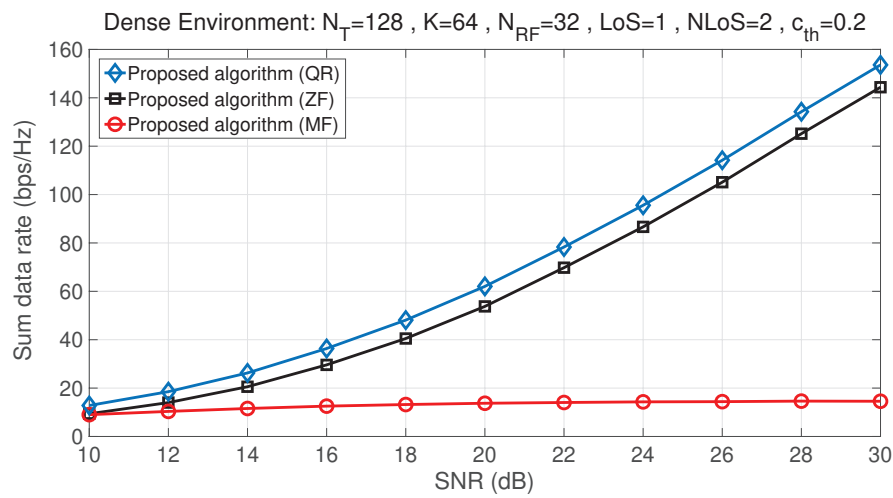

Figure 2.15. Sum data rate results of different precoders for proposed algorithm with 128 antennas, 64 users, 32 RF chains and 2 NLoS components, $c_{th} = 0.2$.

In Figure 2.16, the performance results are demonstrated for different number of users while the number of antennas and RF chains are fixed. As the number of users is increased, the sum data rate results for both algorithms are enhanced for ZF precoder.

In Figure 2.17, the sum data rate results for QR precoder is given for different number of users. The sum data rate is proportional to the number of users for both algorithms although the total number of users is 32. Because, as the number of users is increased, the chance to select well-conditioned users is increased. Therefore, the inter-user interference is decreased.

In Figure 2.18, the simulation is performed for different number of antennas while the number of users and RF chains are fixed and ZF precoder is used. The proposed algorithm with 128 antennas gives almost the same performance of MM algorithm with

256 antennas although it has less number of antennas. Because, MM algorithm is more sensitive to highly correlated user channels. Also, decreasing the number of antennas degrades the performance of MM algorithm much more than proposed algorithm because of the correlation issue. Therefore, the sum data rate of MM algorithm with 128 antennas is quite low.
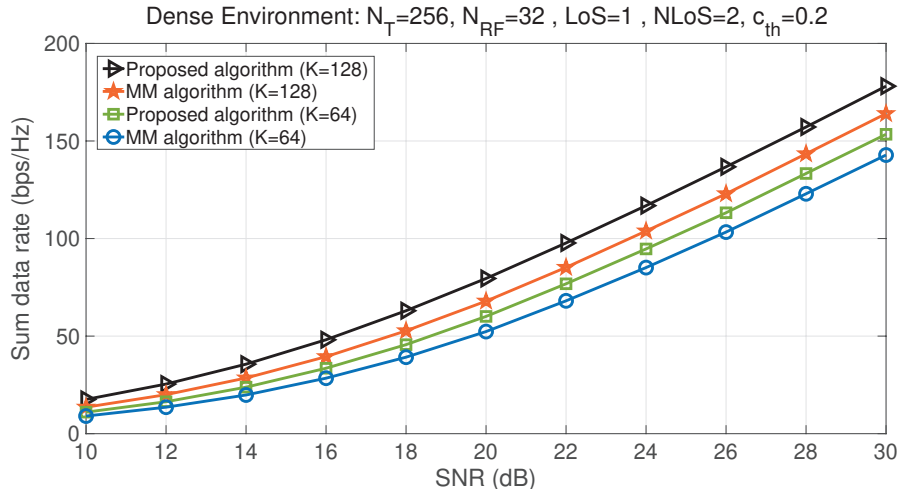

Figure 2.16. Sum data rate results of MM and proposed algorithms for ZF precoder with 256 antennas, 32 RF chains and 2 NLoS components, $c_{th} = 0.2$.
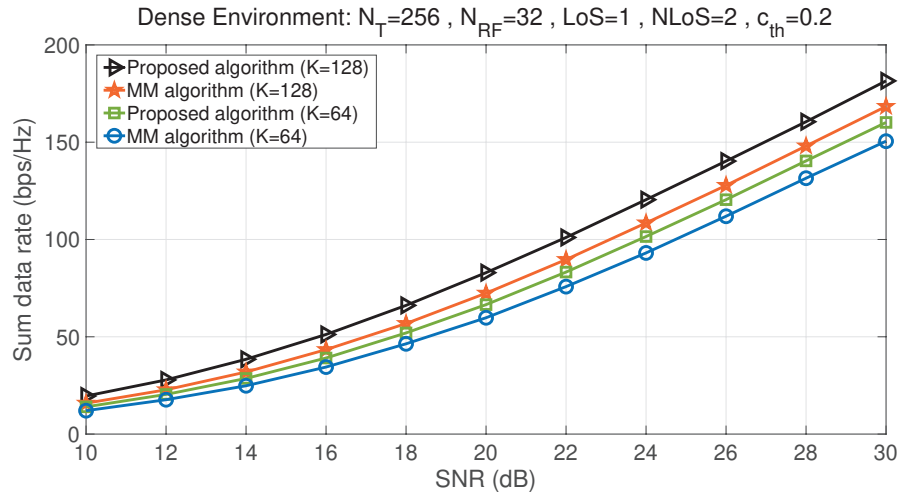

Figure 2.17. Sum data rate results of MM and proposed algorithms for QR precoder with 256 antennas, 32 RF chains and 2 NLoS components, $c_{th} = 0.2$.
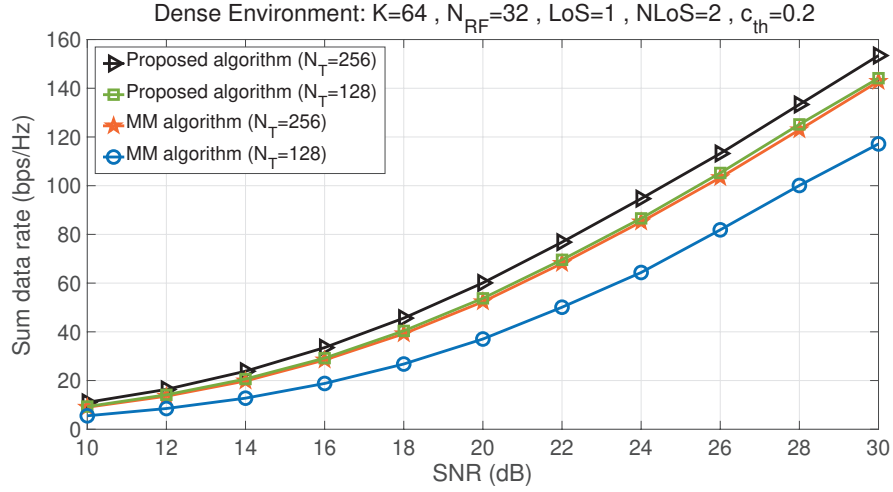
Figure 2.18. Sum data rate results of MM and proposed algorithms for ZF precoder with 64 users, 32 RF chains and 2 NLoS components, $c_{th} = 0.2$.

In Figure 2.19, the performance evaluation is performed for different number of antennas while the number of users and RF chains are fixed and QR precoder is used. As the number of antennas is increased, the sum data rate results of algorithms are enhanced.
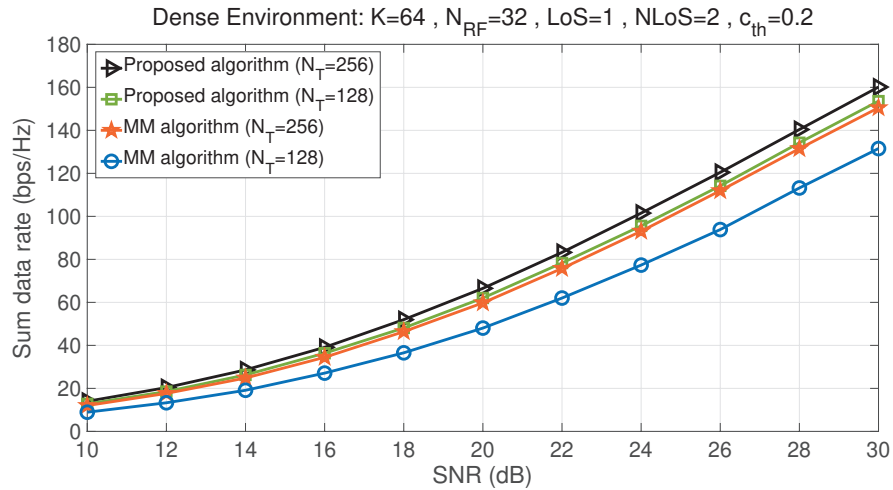
Figure 2.19. Sum data rate results of MM and proposed algorithms for QR precoder with 64 users, 32 RF chains and 2 NLoS components, $c_{th} = 0.2$.

In Figure 2.20, the performance evaluations of MM and proposed algorithms are demonstrated in order to comprehend the effect of the threshold value for ZF precoder. Since the correlated users are eliminated according to the threshold value c_{th}, the performance of the proposed algorithm is dramatically high compared to MM algorithm.

Because, when the correlation between the users is reduced, namely the inter-user interference is mitigated, SINR is increased which increases the sum data rate. When c_{th} is increased, the proposed user selection algorithm eliminates less number of highly correlated users. So, it degrades the performance of the proposed algorithm.
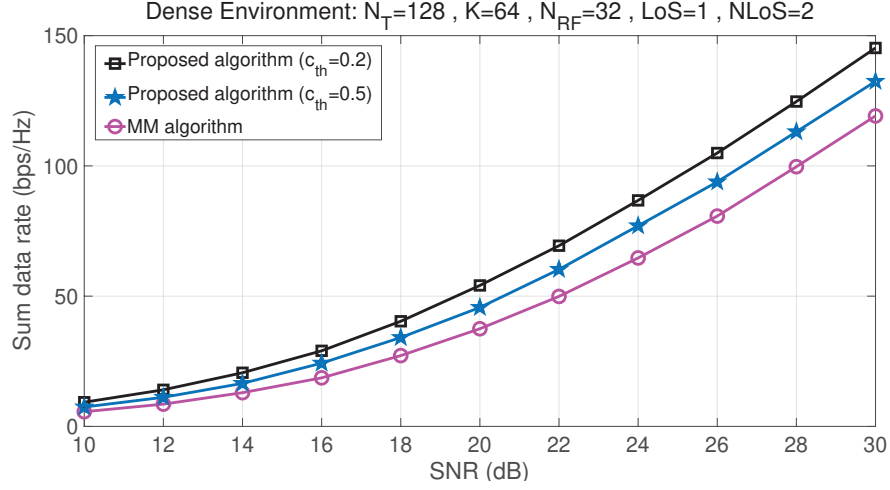

Figure 2.20. Sum data rate results of proposed algorithm with $c_{th} = 0.2$, $c_{th} = 0.5$ and MM algorithm for ZF precoder with 128 antennas, 64 users, 32 RF chains and 2 NLoS components.

In Table 2.1, the average number of selected users and the sum data rates for ZF, MF and QR precoders based on the correlation threshold are demonstrated. As the thresh-

$N_{\mathrm{T}} = 128, K = 64, N_{RF} = 32$			
Threshold value	Precoder type	Sum data rate (bps/Hz)	Number of selected users
$c_{th} = 0.2$	QR	58.57	46.98
	ZF	53.89	
	MF	13.68	
$c_{th} = 0.3$	QR	56.97	51.88
	ZF	51.78	
	MF	13.5	
$c_{th} = 0.4$	QR	55.6	55.42
	ZF	49.37	
	MF	13.4	
$c_{th} = 0.5$	QR	53.81	58.3
	ZF	46.3	
	MF	13.19	

Table 2.1. Comparison of the effect of c_{th} for SNR=20 dB.

old is increased, the average number of selected users is increased and the sum data rates for all precoders are decreased. Thus, as the number of eliminated users increases, the performance of the proposed algorithm is improved.

In Figure 2.21, the sum data rate results are given for 5 NLoS components so that the effect of the number of NLoS components on the system performance can be deduced. It can be distinguished that increasing the number of NLoS components suppresses the positive contribution of the user selection algorithm. Because, the users become less correlated when the number of scatterers increased. Also, it is clearly indicated that the sum data rate results are exactly the same for different threshold values because of low correlation.
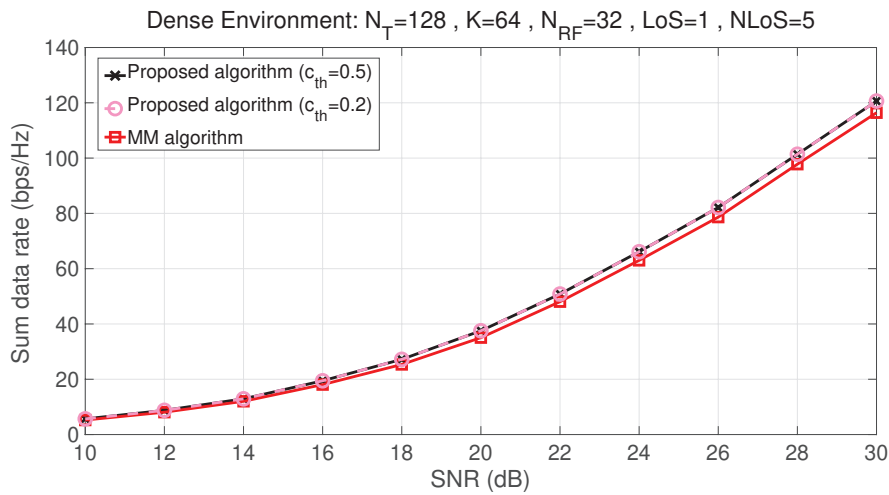

Figure 2.21. Sum data rate results of proposed algorithm with $c_{th} = 0.2$, $c_{th} = 0.5$ and MM algorithm for ZF precoder with 128 antennas, 64 users, 32 RF chains and 5 NLoS components.

In this section, the sum data rate performances of MM and Greedy algorithms have been investigated in various sparse environments including different number of antennas and users. Moreover, the performances of different beamspace precoders such as ZF and MF precoders have been evaluated in such kind of environments. On the other hand, the sum data rate performance of the proposed algorithm have been investigated in several dense environments with different parameters. The performances have been evaluated for ZF, MF and QR precoders. Also, the effects of the threshold value c_{th} and the number of NLoS components on the sum data rate have been examined.

CHAPTER 3

NON-UNIFORM FULL DIMENSIONAL MIMO

Full dimensional MIMO (FD-MIMO) is a special concept that utilizes uniform rectangular array (URA) differently from the conventional MIMO utilizing ULA. Therefore, FD-MIMO realizes 3D spatial channel based on the Kronecker product as in Eq.(3.1) while the conventional MIMO introduces 2D spatial channel as in Eq.(2.12). Also, FD-MIMO makes 3D beamforming achievable, which corresponds to simultaneous beamforming in azimuth and elevation domains. On the other hand, conventional massive MIMO systems utilize uniform linear array (ULA) which enables beamforming only in azimuth domain. As can be seen in the FD-MIMO system in Figure 3.1, beams that serve the users on the ground are formed in horizontal direction (azimuth), and beams for the users in the building are in vertical direction (elevation). Thus, the advantage of more degree of freedom in spatial domain is gained due to rectangular antenna structure.
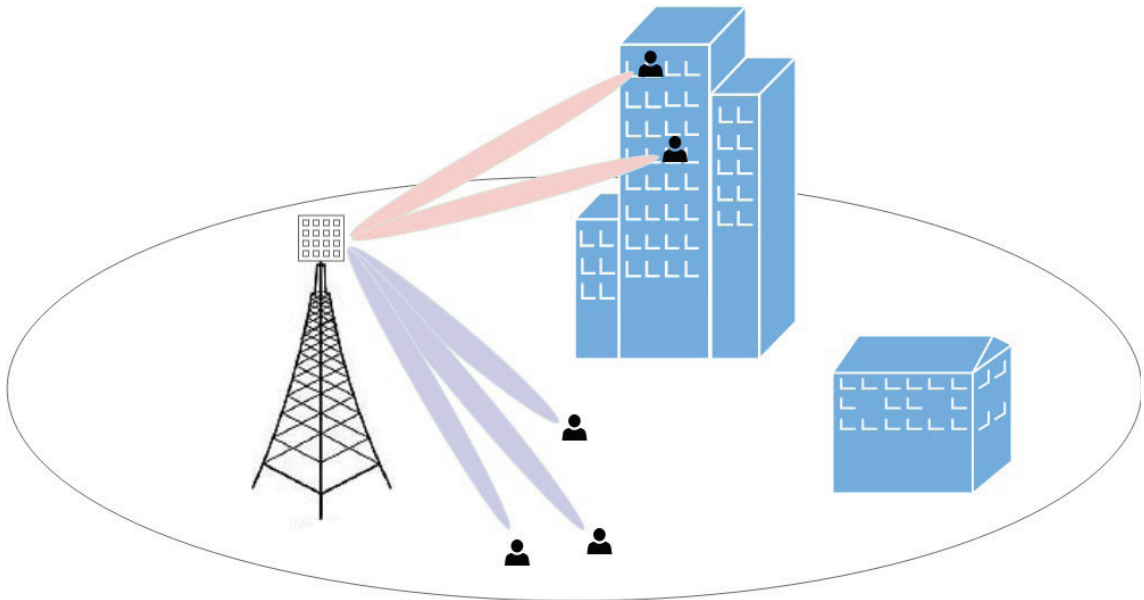

Figure 3.1. FD-MIMO system.

Another superiority of rectangular antenna structure is its compactness which can be critical especially in mmWave massive MIMO systems. For example, considering an

8×8 URA and 1×64 ULA structures, both of them with half wavelength antenna spacing, URA takes up nearly 0.043 meters $\times$ 0.043 meters space at 28 GHz operating frequency while ULA takes up 0.343 meters horizontal space which is a lot more. As the number of antenna elements increases, it will be extremely challenging to implement ULA structure due to the space limitation issue. Therefore, URA is considered as a key solution for this problem. On the other hand, FD-MIMO system utilizing URA is less spectrum efficient than the system which has the same number of antenna elements but in ULA configuration. In order to enhance the spectral efficiency in FD-MIMO, using a non-uniform rectangular array (NURA) which has a non-uniform antenna distribution in elevation domain has been presented in (Liu and Wang, 2019). Figure 3.2 illustrates three different rectangular array configurations according to the uniformity of antenna distributions in vertical direction.
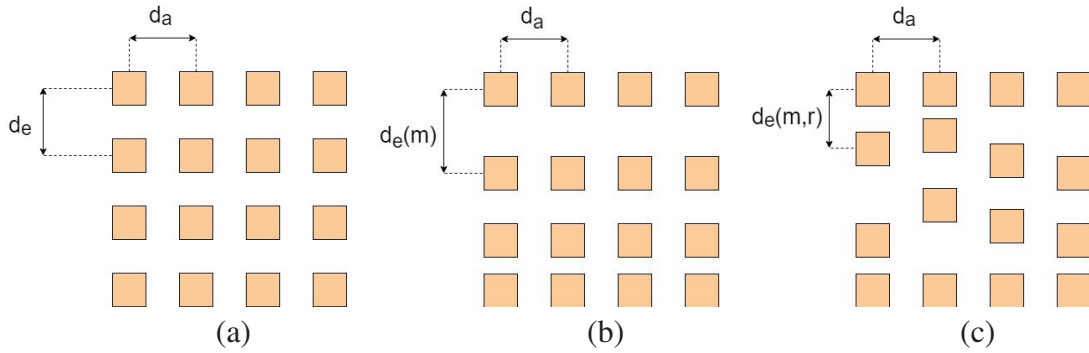

Figure 3.2. Demonstration of 4×4 rectangular array antenna configurations: (a) URA, (b) structured NURA, (c) unstructured NURA.

Figure 3.2(a) shows a conventional URA which has a constant antenna spacings in azimuth and elevation directions which are denoted by d_a and d_e, respectively. In all three configurations, azimuth direction has constant spacing which is generally half-wavelength. But in elevation direction, uniformity can not be mentioned for the configurations in (b) and (c) options of Figure 3.2.

In Figure 3.2(c), an unstructured NURA is demonstrated and antenna spacing in the elevation direction $d_e(m, r)$ is subjected to both row index m and column index r. But for the structured NURA shown in Figure 3.2.(b), $d_e(m)$ depends only on the row index m. In other words, structured NURA has the same layout for each column of antenna elements.

3.1. System Model

In this section, a downlink mmWave communication system based on FD-MIMO is considered. The system contains a BS, which is equipped with $N_e \times N_a$ dimensional rectangular array, N_{RF} RF chains and K single-antenna users. 3D spatial channel model is used for the channel between the BS and the kth user:

$$\mathbf{H}_k = \beta_k^{(0)} \mathbf{a}_e\left(\varphi_k^{(0)}\right) \otimes \mathbf{a}_a^T\left(\vartheta_k^{(0)}, \varphi_k^{(0)}\right) + \sum_{p=1}^{N_p} \beta_k^{(p)} \mathbf{a}_e\left(\varphi_k^{(p)}\right) \otimes \mathbf{a}_a^T\left(\vartheta_k^{(p)}, \varphi_k^{(p)}\right) \qquad (3.1)$$

where $\varphi_k^{(0)}$ and $\varphi_k^{(p)}$ are the elevation AoDs and $\vartheta_k^{(0)}$ and $\vartheta_k^{(p)}$ are the azimuth AoDs for the LoS and p^{th} NLoS components of the kth user, respectively. The channel matrix $\mathbf{H}_k \in \mathbb{C}^{N_e \times N_a}$ is associated with the Kronecker product of the array steering vectors of elevation $\mathbf{a}_e\left(\varphi_k^{(0)}\right) \in \mathbb{C}^{N_e \times 1}$ and of azimuth $\mathbf{a}_a\left(\vartheta_k^{(0)}, \varphi_k^{(0)}\right) \in \mathbb{C}^{N_a \times 1}$ for LoS path, and the array steering vectors of elevation $\mathbf{a}_e\left(\varphi_k^{(p)}\right) \in \mathbb{C}^{N_e \times 1}$ and of azimuth $\mathbf{a}_a\left(\vartheta_k^{(p)}, \varphi_k^{(p)}\right) \in \mathbb{C}^{N_a \times 1}$ for NLoS paths.

For describing the steering vectors, a function which expresses the position of each element in the array is required. In azimuth domain, space between the adjacent antenna elements is determined by $d_a = \lambda/2$. Therefore, the position of the elements are predefined and the steering vector can be expressed by (Nam et al., 2013),(Li et al., 2016):

$$\mathbf{a}_a\left(\vartheta_k^{(p)}, \varphi_k^{(p)}\right) = \frac{1}{\sqrt{N_a}}\left[1, e^{-j2\pi \frac{d_a}{\lambda} sin\vartheta_k^{(p)} cos\varphi_k^{(p)}}, \ldots, e^{-j2\pi \frac{(N_a-1)d_a}{\lambda} sin\vartheta_k^{(p)} cos\varphi_k^{(p)}}\right]^T \qquad (3.2)$$

On the other hand, some methods such as exponent-based, exponential and tangent-based are defined in (Liu et al., 2017) for the elevation domain. Exponent based method describes the function $g_\eta(m)$, depending on m, as below :

$$g_\eta(m) = d_e\left(N_e - 1\right)\left(\frac{m}{N_e - 1}\right)^\eta \qquad (3.3)$$

where $m = 0, \ldots, N_e - 1$. This function offers a non-uniform antenna distributions as in (a) and (c) options of Figure 3.3. Yet in (b), the function $g_{\eta=1}(m) = md_e$ shows a linear

characteristics just like in the azimuth domain. Thus, the array will be URA for the case that provides $\eta = 1$.
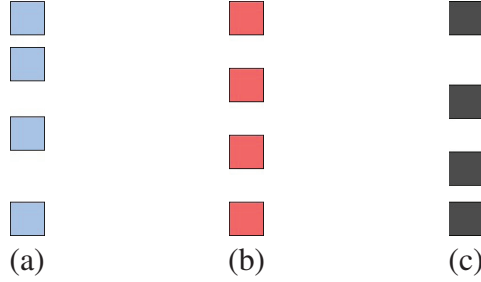

Figure 3.3. Pattern of antenna elements with: (a) $0 < \eta < 1$, (b) $\eta = 1$, (c) $\eta > 1$.

The exponent η can substantially affect the spectral efficiency of the system. Therefore, the exponent that gives the maximum spectral efficiency can be investigated to reach the optimal structured NURA design.

For NURA configurations, there are two types depending on the variability of η. For dynamic NURA, η have to be varied with respect to the channel realization to achieve the maximum sum data rate. Therefore, this provides the optimal structured NURA design. However, the implementation of dynamic NURA requires new manufacturing technologies which enable the reconfiguration of the array. The other type is static NURA in which η is predetermined and does not depend on the instantaneous channel realization. It is determined regarding the several channel realizations and average sum data rate. Thus, it is more favorable and applicable for our system model.

By using the positioning function, the array steering vector in elevation domain can be expressed by:

$$
\mathbf{a}_e\left(\varphi_k^{(p)}\right) = \frac{1}{\sqrt{N_e}}\left[1, e^{-j2\pi \frac{g(1)}{\lambda} sin\varphi_k^{(p)}}, \ldots, e^{-j2\pi \frac{g(N_e - 1)}{\lambda} sin\varphi_k^{(p)}}\right]^T \tag{3.4}
$$

However, because of the small angular spread in the elevation domain, all the paths can be approached to a single path such that $\mathbf{a}_e\left(\varphi_k^{(p)}\right) \approx \mathbf{a}_e(\varphi_k), \forall p$. Therefore, the channel described in Eq.(3.1) can be degraded to:

$$
\mathbf{H}_k \approx \beta_k^{(0)}\mathbf{a}_e\left(\varphi_k^{(0)}\right) \otimes \mathbf{a}_a^T\left(\vartheta_k^{(0)}, \varphi_k^{(0)}\right) + \mathbf{a}_e(\varphi_k) \otimes \sum_{p=1}^{N_p} \beta_k^{(p)}\mathbf{a}_a^T\left(\vartheta_k^{(p)}, \varphi_k\right) \tag{3.5}
$$

36

And, the received signal for the kth user is defined as:

$$r_k = \mathbf{h}_k^H \mathbf{x} + n_k \tag{3.6}$$

where $\mathbf{h}_k \in \mathbb{C}^{N_e N_a \times 1}$ is a vector form of the channel matrix $\mathbf{H}_k$, namely $\mathbf{h}_k = vec(\mathbf{H}_k)$, $\mathbf{x} \in \mathbb{C}^{N_e N_a \times 1}$ denotes the vector of transmitted symbols for all users and n_k is AWGN for the kth user. Thus, the whole system equation can be written as:

$$\mathbf{r} = \mathbf{HWs} + \mathbf{n} \tag{3.7}$$

where $\mathbf{H} = [\mathbf{h}_1, \mathbf{h}_2, \ldots, \mathbf{h}_K]^T \in \mathbb{C}^{K \times N_e N_a}$, the corresponding precoding matrix is denoted by $\mathbf{W} \in \mathbb{C}^{N_e N_a \times K}$, $\mathbf{s} = [s_1, s_2, \ldots, s_K]^T$ is the symbol vector for all users and $\mathbf{n}$ represents the AWGN vector.

For the precoding scheme, $\mathbf{W}$ can be computed directly over $\mathbf{H}$ or by vectorizing $\mathbf{H}$ such that $\acute{\mathbf{h}} = vec(\mathbf{H})$ where $\acute{\mathbf{h}} \in \mathbb{C}^{1 \times K N_e N_a}$. For the ZF precoder, the precoding matrix is determined as:

$$\mathbf{W} = \alpha \mathbf{H}^H \left(\mathbf{HH}^H\right)^{-1} \tag{3.8}$$

The scaling factor is then computed by:

$$\alpha = \sqrt{\frac{\rho}{tr\left(\left(\mathbf{HH}^H\right)^{-1}\right)}} \tag{3.9}$$

where ρ is the total transmit power.

3.2. Proposed User Selection Algorithm

Since the number of antennas is low, the conventional digital MIMO architecture is utilized as seen in Figure 3.4. Therefore, the relation between the number of antennas

37

and RF chains is $N_{\mathrm{RF}} = N_{\mathrm{T}}$ where $N_{\mathrm{T}} = N_e \times N_a$. On the other hand, the system contains more users than the RF chains, $K > N_{\mathrm{RF}}$ in the dense environment. However, the number of users that can be served by the system is N_{RF} at most and $(K - N_{\mathrm{RF}})$ users must be eliminated while maximizing the sum data rate. A decremental user selection algorithm (Cumalı, Özbek, Mumtaz, and Gonzalez, 2020) is proposed so that the maximum number of users can be served while achieving the maximum sum data rate.
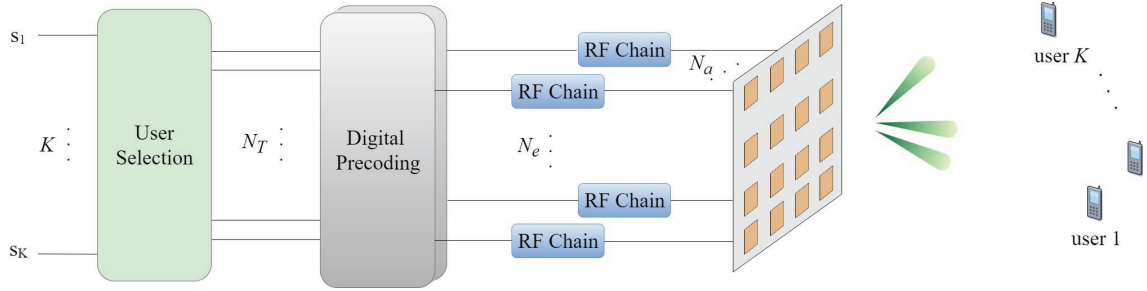

Figure 3.4. Transceiver architecture for FD-MIMO in the dense environment.

For this system, the proposed algorithm evaluates the correlation between all K users. Based on the correlations, the proposed algorithm eliminates $(K - N_{\mathrm{RF}})$ users in $(K - N_{\mathrm{RF}})$ iterations. The rows of the spatial channel matrix $\mathbf{H}$ in Eq.(3.7) presents the users' channels. Therefore, the correlation between i^{th} and j^{th} user is described by:

$$c(i,j) = \frac{|\mathbf{H}(i,:)^H \mathbf{H}(j,:)|}{\|\mathbf{H}(i,:)\| \|\mathbf{H}(j,:)\|} \tag{3.10}$$

At each iteration, the proposed algorithm calculates the correlation matrix $\mathbf{C}$ whose $(i,j)^{th}$ element $\mathbf{C}_{i,j}$ is equal to $c(i,j)$. Then, the user pair $\kappa = (\kappa_1, \kappa_2)$ that has the maximum correlation value is determined over $\mathbf{C}$. In this pair, the user that has the lowest channel gain is eliminated. Finally, the resulting matrix $\hat{\mathbf{H}}$ that has lower dimension is constituted by ejecting the channel vector of that user from the channel matrix. The number of rows n_r, which is initially equal to K, is redetermined at each iteration and the proposed algorithm continues to eliminate a user until there are N_{RF} users left, meaning that n_r in the last iteration is equal to N_{RF}. In Figure 3.5, the proposed algorithm is provided. After the proposed algorithm is applied, the precoding is performed over the resulting channel matrix $\hat{\mathbf{H}}$ by using Eq.(3.8) and Eq.(3.9).

Algorithm 1: Proposed decremental user selection algorithm

Input: $\mathbf{H} \in \mathbb{C}^{K \times N_e N_a}$
Initialize: $\hat{\mathbf{H}} = \mathbf{H}, n_r = K$;
while $n_r > N_{\mathrm{RF}}$ **do**
    $\mathbf{C} = \mathbf{0}_{n_r \times n_r}$;
    for $i = 1 \rightarrow n_r$ **do**
        for $j = i \rightarrow n_r$ **do**
            $\mathbf{C}_{i,j} = \mathrm{c}(i,j)$;
        end
    end
    Find (κ_1, κ_2) such that $\mathbf{C}_{\kappa_1, \kappa_2} = \max(\mathbf{C})$ where $\kappa_1 \neq \kappa_2$;
    if $\left\| \hat{\mathbf{H}}(\kappa_1, :) \right\| \leq \left\| \hat{\mathbf{H}}(\kappa_2, :) \right\|$ **then**
        Eliminate κ_1^{th} user channel from $\hat{\mathbf{H}}$;
    else
        Eliminate κ_2^{th} user channel from $\hat{\mathbf{H}}$;
    end
    $[n_r, n_c] = size(\hat{\mathbf{H}})$;
end
Output: $\hat{\mathbf{H}} \in \mathbb{C}^{N_{\mathrm{RF}} \times N_e N_a}$

Figure 3.5. Proposed decremental algorithm for user selection.

From the point of complexity, our algorithm computes the correlation matrix in each iteration out of $(K - N_{\mathrm{RF}})$ total iterations. On the other hand, selection of the users with highest channel norm, which is used for the performance comparisons in Section 3.3.2, computes the channel norms of all users in each iteration and selects the users in N_{RF} iterations. Therefore, the complexity of our algorithm is reasonable.

3.3. Performance Evaluations

For the FD-MIMO in Eq.(3.7), the performance evaluations of URA and NURA structures using ZF precoding scheme are performed. The simulation environment contains K users served by an $N_e \times N_a$ dimensional rectangular array antenna.

For the sparse environment which has $K \leq N_{\mathrm{RF}} = N_{\mathrm{T}}$, it is aimed to evaluate the performances of URA and structured NURA configurations with the same number of antenna in azimuth and elevation domains. Also, sum data rate performances of rectangular array configurations depending on the exponent η is investigated to conclude the optimal NURA design for a specific antenna dimensions.

For the dense environment which has $K > N_{\mathrm{RF}} = N_{\mathrm{T}}$, the performance evalua-

tions of the proposed user selection algorithm for different number of antennas in elevation and azimuth directions are demonstrated. For the kth user, the channel matrix $\mathbf{H}_k$ in Eq.(3.5) has the parameters given in the following:

- $\beta_k^{(0)} \sim \mathcal{CN}(0, 1)$ for LoS component,
- Elevation AoD $\varphi_k^{(0)} \sim \mathcal{U}(-90, +90)$ for LoS component,
- Azimuth AoD $\vartheta_k^{(0)} \sim \mathcal{U}(-90, +90)$ for LoS component,
- $\beta_k^{(p)} \sim \mathcal{CN}(0, 0.1)$ when $p = 1, 2$.
- Elevation AoD $\varphi_k^{(p)} \sim \mathcal{U}(\varphi_k^{(0)} - \delta_e/2 \, , \, \varphi_k^{(0)} + \delta_e/2)$ for only an NLoS, where the

angular spread of elevation δ_e is 6 degrees.

- Azimuth AoDs $\vartheta_k^{(p)} \sim \mathcal{U}(\vartheta_k^{(0)} - \delta_a/2 \, , \, \vartheta_k^{(0)} + \delta_a/2)$ for $p = 1, 2$, where the

angular spread of azimuth δ_a is 180 degrees.

3.3.1. Simulation Results for FD-MIMO in Sparse Environment

Figure 3.6 demonstrates the performance of 4×2 array antenna for different values of exponent η for SNR=10 dB and SNR=30 dB. The highest sum data rate is obtained when η=0.65 while the minimum is obtained when η=0 for both SNR values. If η=1, the configuration corresponds to URA. Therefore, for η values between 0.25 and 2 except for η=1, all NURA configurations achieve better sum data rate performances than URA that has sum data rate of 20 bps/Hz at 30 dB and 2 bps/Hz at 10 dB.
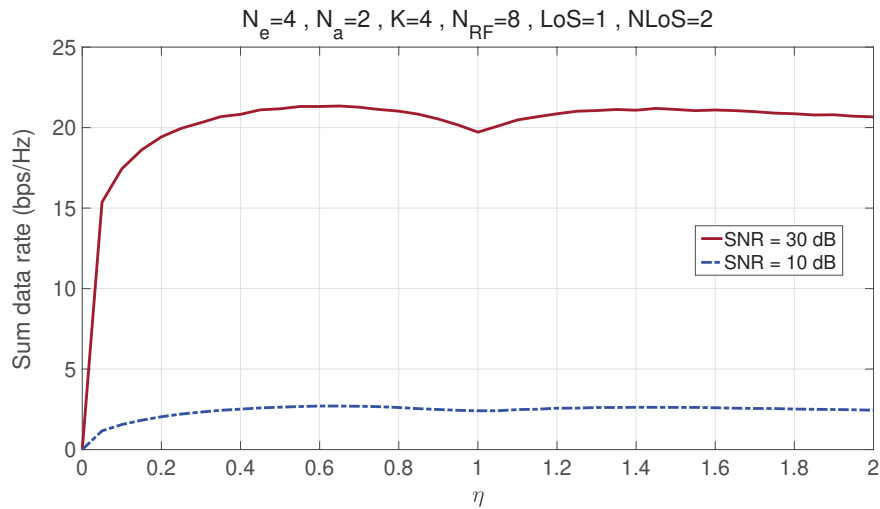

Figure 3.6. Sum data rate versus η for 4×2 array with 4 users at SNR=10 dB and SNR=30 dB.

Figure 3.7 shows that 4×2 structured NURA with the exponent of 0.65 outperforms 4×2 URA for all SNR values. The sum data rate reaches 22 bps/Hz for NURA when SNR is 30 dB. There is approximately 2 bps/Hz sum data rate difference of between URA and NURA.
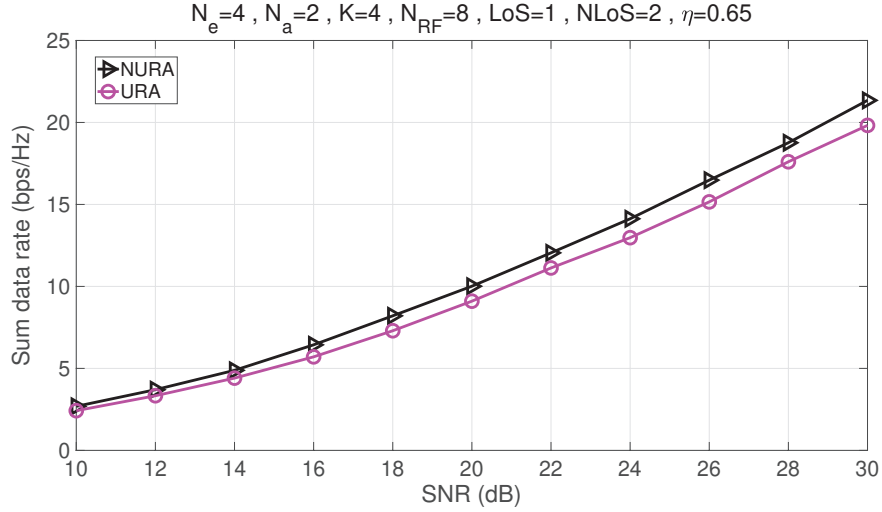

Figure 3.7. Sum data rate results of 4×2 URA and NURA with 4 users, η=0.65.

In Figure 3.8, the performance of 4×2 array antenna with respect to the exponent η is illustrated when K=6 and SNR=30 dB. For η values greater than 0.3, all NURA
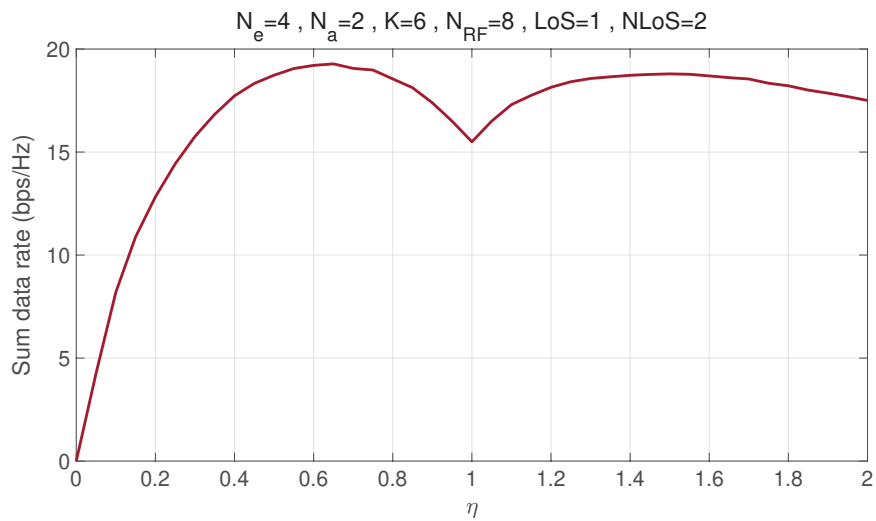
Figure 3.8. Sum data rate versus η for 4×2 array with 6 users at SNR=30 dB.

configurations achieve better sum data rate performances than URA which has sum data rate of 15.5 bps/Hz at 30 dB. Then, the optimal η value is determined as 0.65.

In Figure 3.9, the sum data rate comparison is demonstrated when η is determined as 0.65. For SNR=30 dB, there is a 4 bps/Hz sum data rate difference between URA and NURA. The difference becomes lower for lower SNR values.
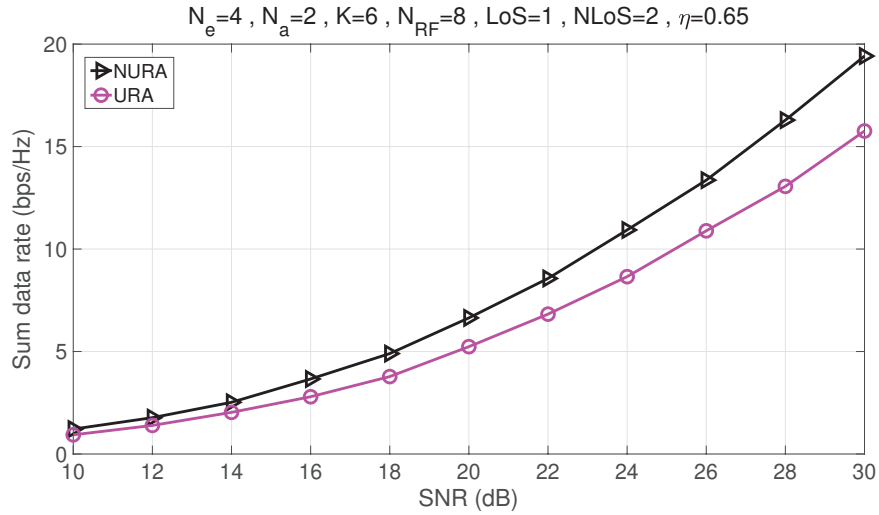

Figure 3.9. Sum data rate results of 4×2 URA and NURA with 6 users, η=0.65.

In Figure 3.10, the performance of 4×4 array antenna with respect to the exponent η is illustrated when the number of user K=8,10,12 at SNR=30 dB. The results indicate

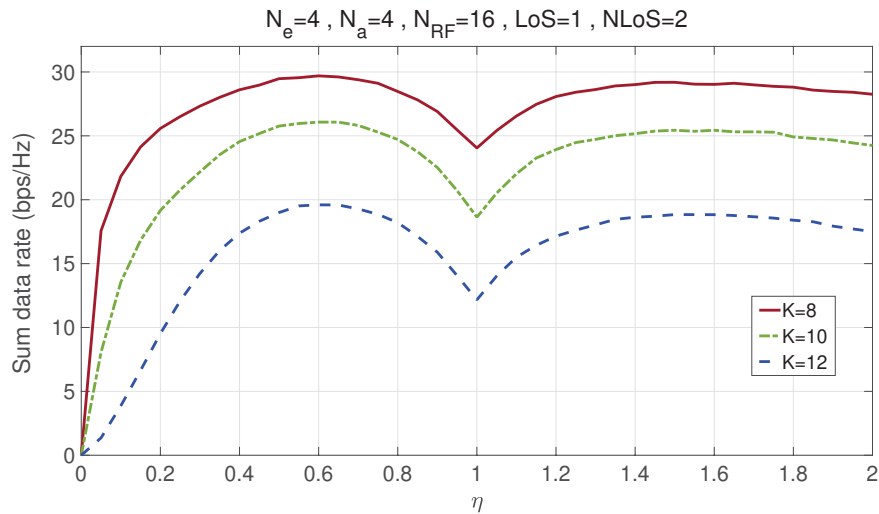Figure 3.10. Sum data rate versus η for 4×4 array for K=8,10,12 at SNR=30 dB.

that the sum data rates of the NURA configurations with the exponent $0.15 \leq \eta \leq 2$ for K=8, $0.20 \leq \eta \leq 2$ for K=10 and $0.25 \leq \eta \leq 2$ for K=12 are greater than their URA counterpart whose exponents are η=1 for all K values. It is remarkable that for the different number of users, the optimal η value is approximately 0.65. Supporting nearly stable η value is a significant property of optimized NURA. Therefore, optimized 4×4 NURA configuration is practicable regardless of the number of users.

In Figure 3.11, the performance evaluation is provided for 4×4 URA and NURA with different number of users and 16 RF chains. As the number of users K is increased, meaning that the correlations between the users' channels is getting higher, the sum data rate results for both URA and NURA are decreased. On the other hand, the sum data rate difference between URA and NURA is enhanced as K increased.
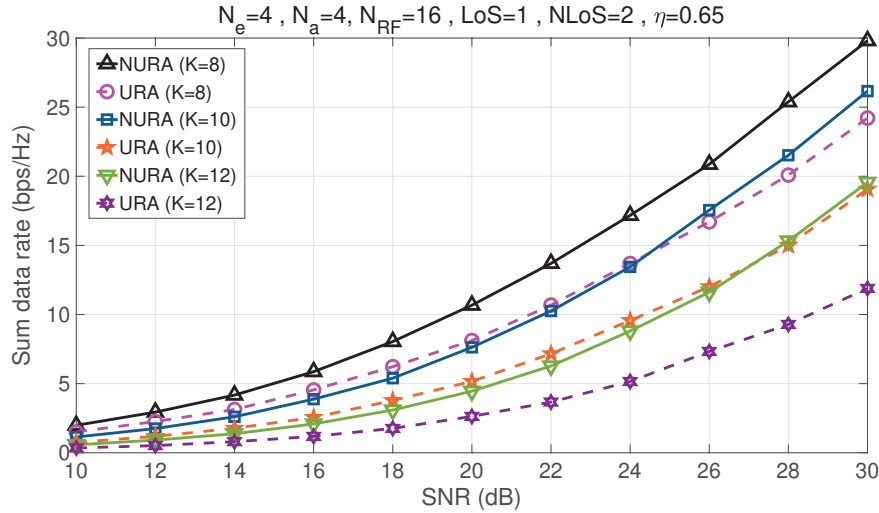

Figure 3.11. Sum data rate results of 4×4 URA and NURA for K=8,10,12 and η=0.65.

In Figure 3.12, performance of 8×4 array antenna with respect to the exponent η is illustrated when K=16 and SNR=30 dB. It is indicated that the maximum sum data rate is obtained when the exponent η=0.75.

In Figure 3.13, performance of 4×8 array antenna with respect to the exponent η is illustrated when K=16 and SNR=30 dB. It is indicated that the maximum sum data rate is obtained when the exponent η is approximately 0.60.

Figure 3.14 illustrates the sum data rate comparison of the systems with 4×8 and 8×4 array antennas. These systems utilizing digital beamformers have equal number of RF chains and equal number of users. Also, their optimized η values obtained from Figure 3.12 and Figure 3.13 are used. The sum data rate results demonstrate that opti-

mized 4×8 NURA configuration provides the best performance. When the number of antenna in the elevation domain is greater than that in the azimuth domain, the correlation between the user channels are much higher. Therefore, the performance is degraded.

In Figure 3.15, the sum data rate results of 4×8 URA and NURA structures are provided for different number of users. While decreasing the number of users, the sum data rate is increasing for both URA and NURA. Therefore, when the system serves the maximum number of users which is equal to N_{RF}, the system provides the lower performance. On the other hand, NURA overcomes URA for all number of users.
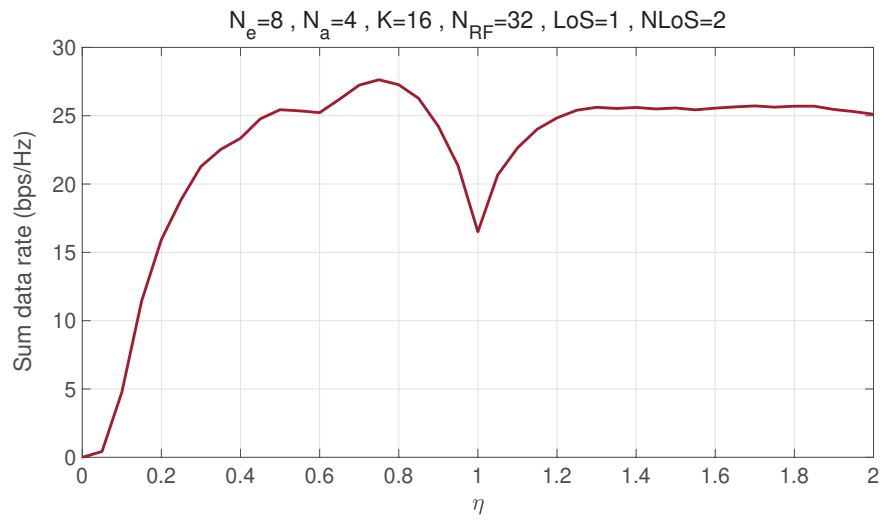

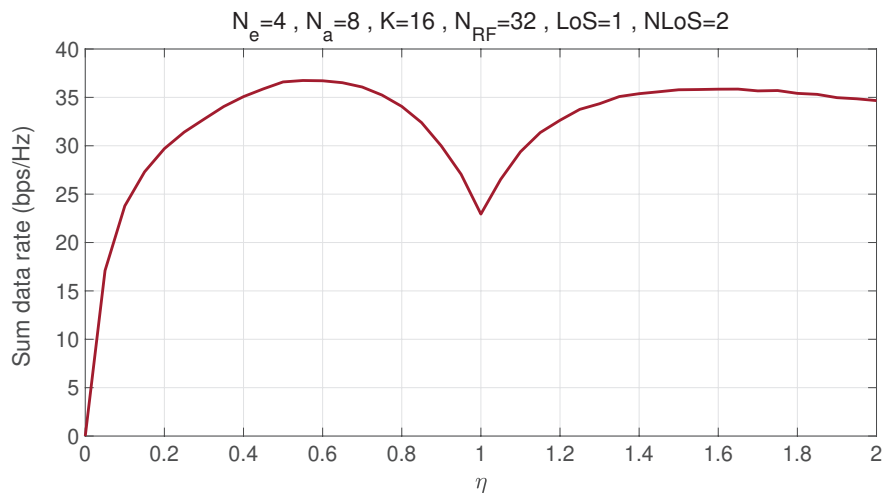Figure 3.12. Sum data rate versus η for 8×4 array with 16 users at SNR=30 dB.

Figure 3.13. Sum data rate versus η for 4×8 array with 16 users at SNR=30 dB.
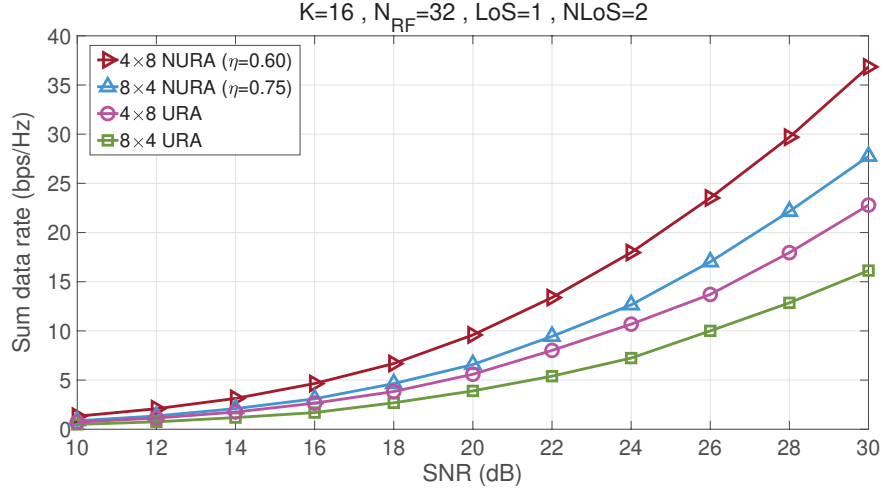
Figure 3.14. Sum data rate results of 4×8 and 8×4 arrays with 16 users.
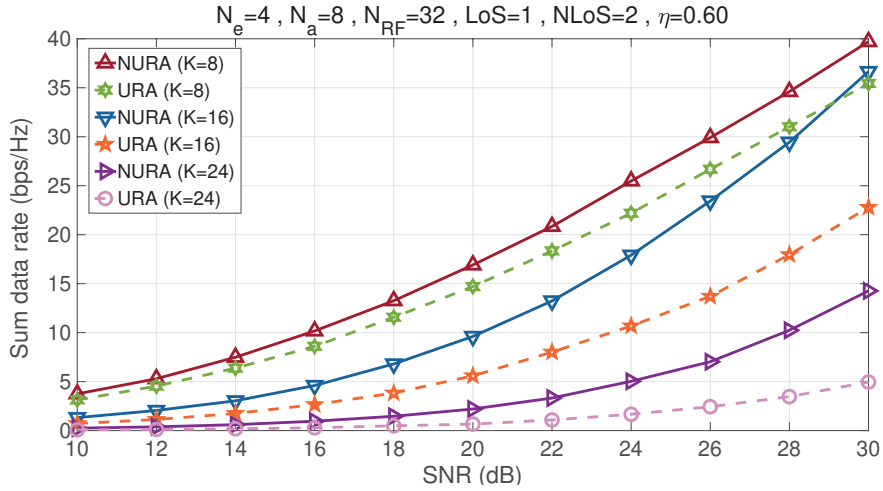

Figure 3.15. Sum data rate results of 4×8 URA and NURA for K=8,16,24 and η=0.60.

3.3.2. Simulation Results for FD-MIMO in Dense Environment

In this section, the simulation environment contains large number of users which is greater than the number of antennas. Therefore, the proposed user selection algorithm is applied to select N_{RF} users among K users. The performance of the proposed algorithm is compared to the performance with random user selection and the users with highest channel norm. In Figure 3.16, the simulation environment contains 4×2 array antenna with 12 users. So, it is required to eliminate 4 users. As shown in the figure, the proposed

45

algorithm enhances the performance of both URA and NURA. On the other hand, NURA still provides higher sum data rate than URA when the proposed user selection is applied.
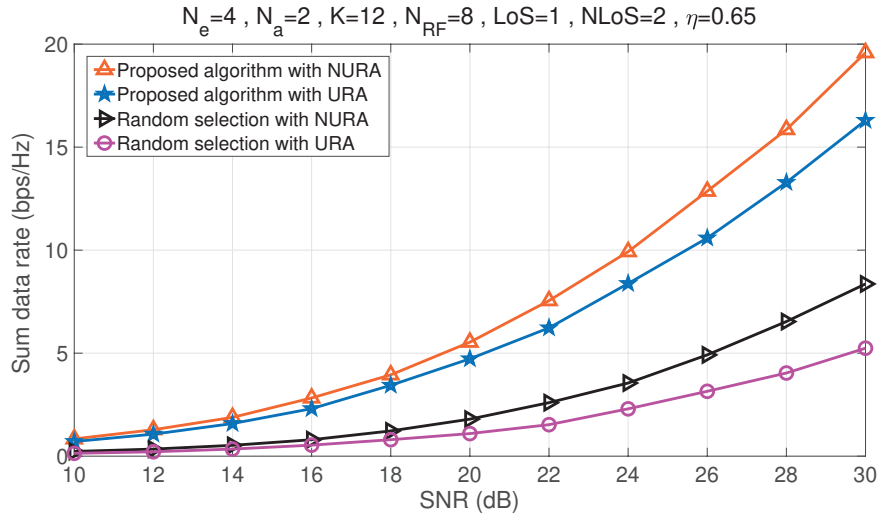

Figure 3.16. Sum data rate results of the proposed user selection algorithm and random user selection with 4×2 URA and NURA, K=12, η=0.65.

In Figure 3.17, the simulation environment contains 4×4 array antenna with 24 users. The optimal η is also determined as 0.65. As in the previous figure, the proposed user selection algorithm provides quite better performance than random user for both URA and NURA. For example, the proposed algorithm with NURA overcomes the
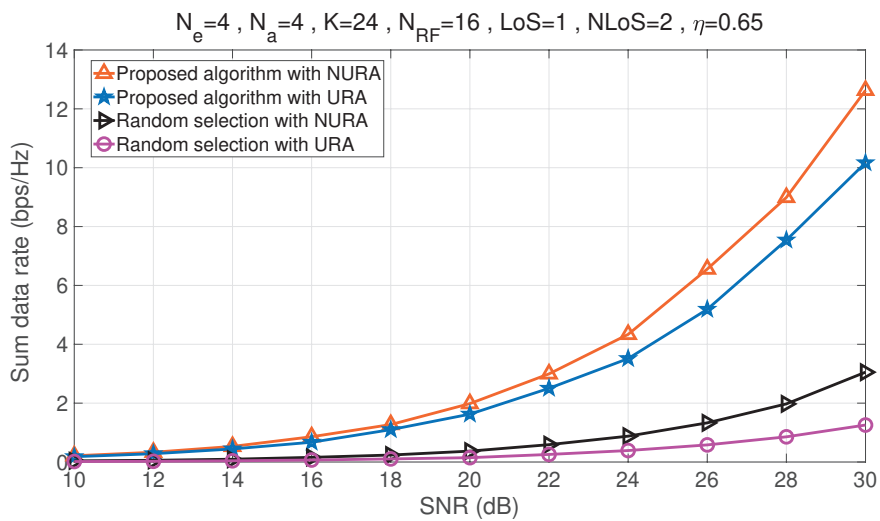

Figure 3.17. Sum data rate results of the proposed user selection algorithm and random user selection with 4×4 URA and NURA, K=24, η=0.65.

random selection with NURA by approximately 9 bps/Hz at SNR=30 dB.

In Figure 3.18, the performance evaluation is obtained for 4×8 array antenna with 48 users. The proposed user selection provides 3 bps/Hz higher sum data rate for NURA configuration at SNR=30 dB. On the other hand, it provides nearly 2.6 bps/Hz higher sum data rate for URA configuration at SNR=30 dB.
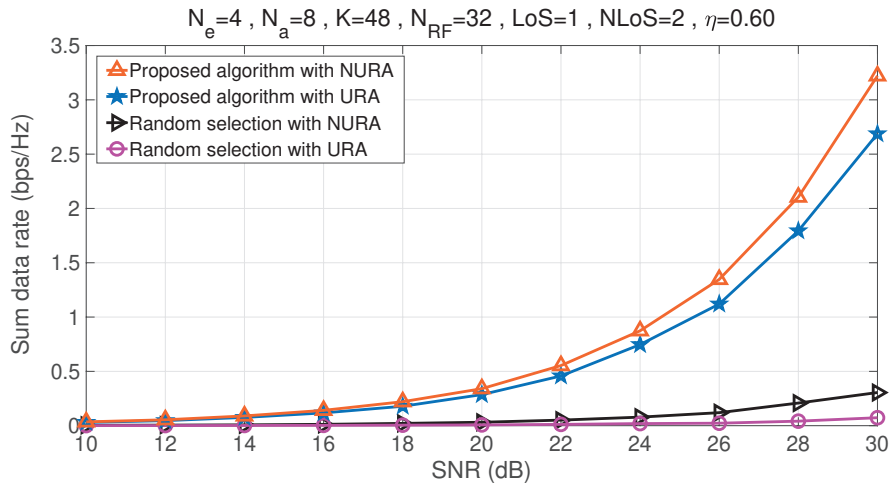

Figure 3.18. Sum data rate results of the proposed user selection algorithm and random user selection with 4×8 URA and NURA, K=48, η=0.60.
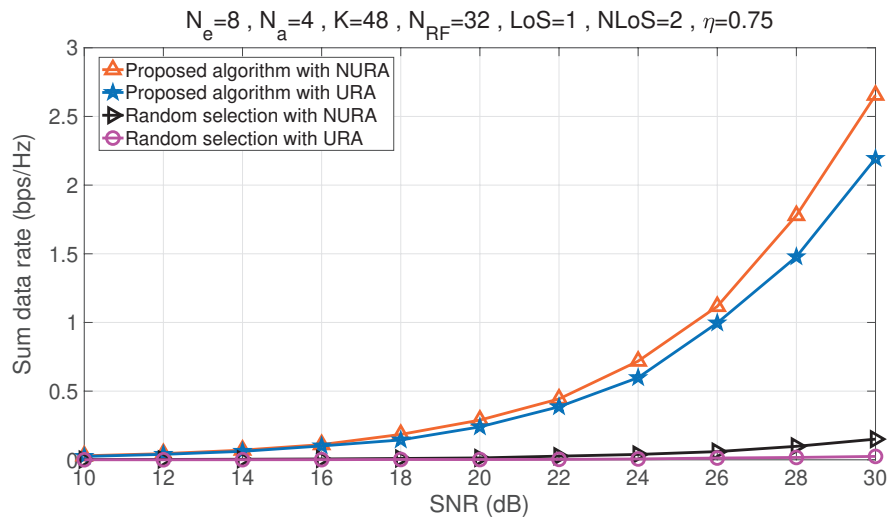

Figure 3.19. Sum data rate results of the proposed user selection algorithm and random user selection with 8×4 URA and NURA, K=48, η=0.75.

In Figure 3.19, the sum data rate result is given for 8×4 array antenna with 64 users.

The proposed user selection algorithm dramatically enhances the sum data rate by eliminating highly correlated user channels especially for NURA.

For the following figures, the performance of the proposed user selection algorithm is compared with the user selection based on the channel norm of the users. For this purpose, N_{RF} users that have higher channel norm are selected.

In Figure 3.20, the performance evaluations are carried out when there are $4{\times}2$ array antenna with 12 users. The comparison is given for the optimized value of NURA structure, which is $\eta = 0.65$. The figure demonstrates that the performance of the proposed algorithm outperforms the performance of the case when the users having higher channel norms are selected.
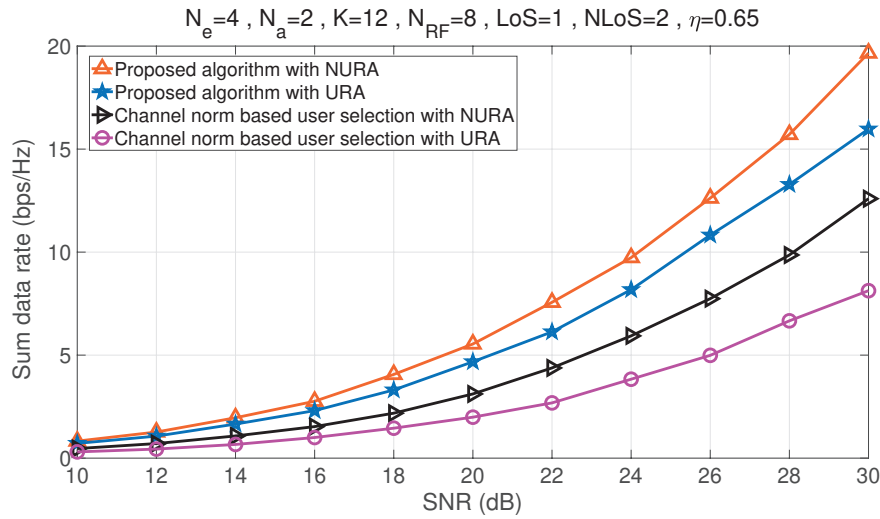

Figure 3.20. Sum data rate results of the proposed user selection algorithm and channel norm based user selection with $4{\times}2$ URA and NURA, K=12, η=0.65.

Figure 3.21 demonstrates the sum data rate performance when there are $4{\times}4$ array antenna with 24 users. The proposed algorithm provides nearly 8 bps/Hz higher sum data rate for both URA and NURA with channel norm based user selection.

The performance results of $4{\times}8$ array antenna with 48 users are provided in Figure 3.22. It demonstrates that the proposed algorithm outperforms the channel condition based selection for both URA and NURA structures.

In Figure 3.23, sum data rate results are given for the optimized value η=0.75 for $8{\times}4$ array antenna when there are 48 users. For this configuration of NURA and URA, the proposed algorithm gives better sum data rate performances.

In Figure 3.24, sum data rate results are given for the proposed algorithm with 4×2, 4×4, 4×8 and 8×4 NURA when there are 48 users. The proposed algorithm selects different number of users depending on the number of antennas. The sum data rate results show that 4x2 NURA structure provides the best performance.

Figure 3.21. Sum data rate results of the proposed user selection algorithm and channel norm based user selection with 4×4 URA and NURA, K=24, η=0.65.

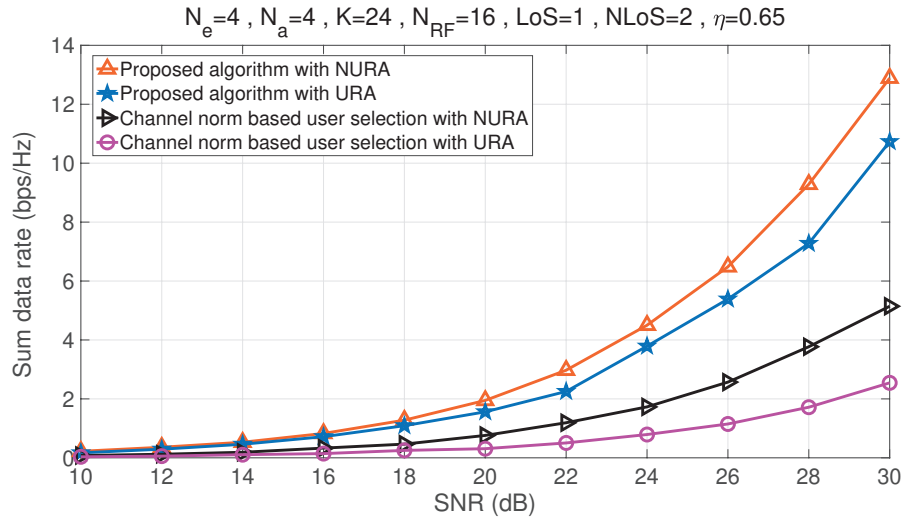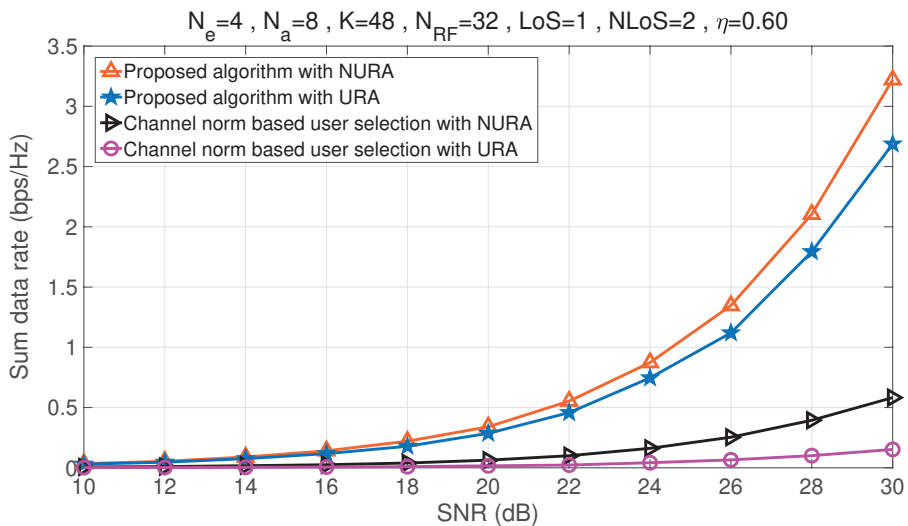

Figure 3.22. Sum data rate results of the proposed user selection algorithm and channel norm based user selection with 4×8 URA and NURA, K=48, η=0.60.
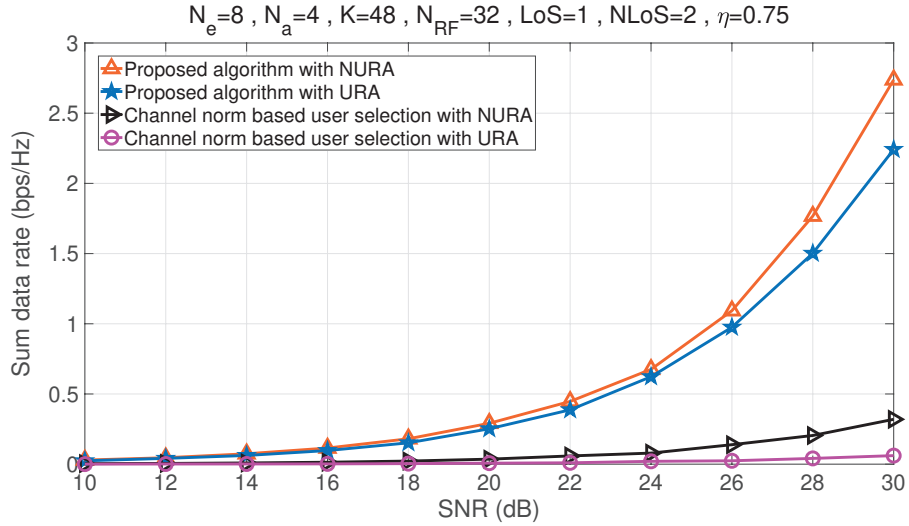
Figure 3.23. Sum data rate results of the proposed user selection algorithm and channel norm based user selection with 8×4 URA and NURA, K=48, η=0.75.
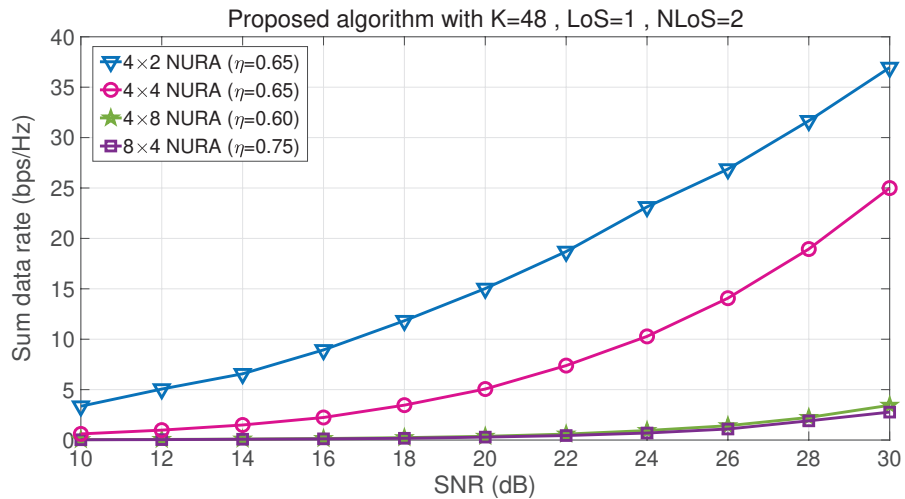
Figure 3.24. Sum data rate results of the proposed user selection algorithm with different NURA structures, K=48.

In this section, the NURA structures have been investigated for mmWave FD-MIMO systems. In the literature, different structured NURA configurations such as dynamic configured and static configured are introduced for FD-MIMO systems operating in sub-6 GHz. This section has adapted the structured NURA configuration to mmWave communications. Accordingly, the 3D channel defined in the literature has been adapted to the mmWave system. On the other hand, the exponent η has optimized for different scenarios containing different number of antennas and users. It has been indicated that

NURA with an optimized η value provides better sum data rate than its URA counterpart. For a system providing a fully digital transceiver architecture with $K > N_{\mathrm{RF}}$, a decremental user selection algorithm based on the correlations of users' channels has been proposed. It has been illustrated that the proposed user selection algorithm has a remarkable improvement on the sum data rate performances of both uniform and non-uniform antenna structures compared to the random user selection and the user selection based on the channel norms.

CHAPTER 4

CONCLUSION

In this thesis, the multi user mmWave communication system has been examined for two different environments called as sparse and dense.

For the sparse environment, the sum data rate performances of MM and Greedy algorithms in the literature have been evaluated under the usage of different beamspace precoders such as ZF and MF. The sum data rate results demonstrate that the Greedy algorithm provides better spectral efficiency than MM algorithm since the number of selected beams in Greedy algorithm is greater than or equal to that in MM algorithm.

On the other hand, the system can not serve all the users in a dense environment on the contrary to the sparse environment. Because there are less number of RF chains compared to the number of users and the maximum number of users that can be served is equal to the number of RF chains. Therefore, user elimination have to be carried out regarding the system performance. It is possible to increase the sum data rate by eliminating the users which have higher correlation. For this purpose, we have proposed the beam and user selection. In the algorithm, the users are selected depending on a threshold value and the beam selection is performed over the degraded and less correlated channel matrix. Thus, not only the sum data rate performance is enhanced but also the complexity of the beam selection algorithm is reduced. Furthermore, the effects of the threshold value on the system performance have been examined and sum data rate results indicate that using a smaller threshold value provides better performance.

Full dimensional MIMO systems have been also investigated. Full dimensional refers to a 3D channel originated from the utilization of 2D array antenna structures. In addition to the conventional uniform rectangular arrays, non-uniform rectangular arrays have been analysed for the millimeter wave system. The performance evaluations have been indicated that the non-uniform structure outperforms its uniform counterpart for different communication environments including different number of users and antennas. Furthermore, the optimal value of the antenna exponent for different environments have been investigated to achieve the optimal antenna design.

We have proposed the decremental user selection algorithm when the system contains higher number of users than the number of antennas for this system employing a digital beamforming architecture. In the proposed algorithm, one user is eliminated in

each iteration and ultimately as many users as the number of RF chains are served in the system. This algorithm has been applied to uniform and non-uniform antenna structures. The sum data rate results indicates that the proposed user selection algorithm increases the spectral efficiency with the non-uniform antenna structure.

As a future work, the proposed user and beam selection algorithm will be applied for a cell-free massive MIMO system. This system contains several number of access points and user equipments in a wide area without the concept of cell. The number of access points is much higher than the number of user equipments in a cell-free massive MIMO system. Therefore, there is not only inter-user interference but also inter-cell interference while the users are served over the same time/frequency resource.

REFERENCES

Alkhateeb, A., J. Mo, N. Gonzalez-Prelcic, and R. W. Heath (2014). Mimo precoding and combining solutions for millimeter-wave systems. *IEEE Communications Magazine 52*(12), 122–131.

Amadori, P. V. and C. Masouros (2015). Low rf-complexity millimeter-wave beamspace-mimo systems by beam selection. *IEEE Transactions on Communications 63*(6), 2212–2223.

Bogale, T. E., L. B. Le, A. Haghighat, and L. Vandendorpe (2016). On the number of rf chains and phase shifters, and scheduling design with hybrid analog–digital beamforming. *IEEE Transactions on Wireless Communications 15*(5), 3311–3326.

Brady, J., N. Behdad, and A. M. Sayeed (2013). Beamspace mimo for millimeter-wave communications: System architecture, modeling, analysis, and measurements. *IEEE Transactions on Antennas and Propagation 61*(7), 3814–3827.

Colon, D. L., F. H. Gregorio, and J. Cousseau (2015). Linear precoding in multi-user massive mimo systems with imperfect channel state information. In *2015 XVI Workshop on Information Processing and Control (RPIC)*, pp. 1–6. IEEE.

Cumalı, I., B. Özbek, R. Mumtaz, and J. Gonzalez (2020). User selection for millimeter wave non-uniform full dimensional mimo. Submitted to IEEE Communications Letters.

Cumalı, I., B. Özbek, and A. Pyattaev (2020). Beam and user selection techniques in millimeter wave communications. Accepted to 2020 IEEE Vehicular Technology Conference (VTC), Antwerp, Belgium.

Gao, X., L. Dai, Z. Chen, Z. Wang, and Z. Zhang (2016). Near-optimal beam selection for beamspace mmwave massive mimo systems. *IEEE Communications Letters 20*(5), 1054–1057.

Heath, R. W., N. Gonzalez-Prelcic, S. Rangan, W. Roh, and A. M. Sayeed (2016). An

overview of signal processing techniques for millimeter wave mimo systems. *IEEE journal of selected topics in signal processing 10*(3), 436–453.

Hegde, A. and K. Srinivas (2019). Matching theoretic beam selection in millimeter-wave multi-user mimo systems. *IEEE Access 7*, 25163–25170.

Joham, M., W. Utschick, and J. A. Nossek (2005). Linear transmit processing in mimo communications systems. *IEEE Transactions on signal Processing 53*(8), 2700–2712.

Li, X., S. Jin, H. A. Suraweera, and X. Gao (2016). Line-of-sight based statistical 3d beamforming for downlink massive mimo systems. In *2016 IEEE International Conference on Communications (ICC)*, pp. 1–6. IEEE.

Liu, W. and Z. Wang (2019). Non-uniform full-dimension mimo: New topologies and opportunities. *IEEE Wireless Communications 26*(2), 124–132.

Liu, W., Z. Wang, C. Sun, S. Chen, and L. Hanzo (2017). Structured non-uniformly spaced rectangular antenna array design for fd-mimo systems. *IEEE Transactions on Wireless Communications 16*(5), 3252–3266.

Nam, Y.-H., B. L. Ng, K. Sayana, Y. Li, J. Zhang, Y. Kim, and J. Lee (2013). Full-dimension mimo (fd-mimo) for next generation cellular technology. *IEEE Communications Magazine 51*(6), 172–179.

Pal, R., A. K. Chaitanya, and K. Srinivas (2019). Low-complexity beam selection algorithms for millimeter wave beamspace mimo systems. *IEEE Communications Letters 23*(4), 768–771.

Pal, R., K. Srinivas, and A. K. Chaitanya (2018). A beam selection algorithm for millimeter-wave multi-user mimo systems. *IEEE Communications Letters 22*(4), 852–855.

Peel, C. B., B. M. Hochwald, and A. L. Swindlehurst (2005). A vector-perturbation technique for near-capacity multiantenna multiuser communication-part i: channel inversion and regularization. *IEEE Transactions on Communications 53*(1), 195–202.

Qiu, S., K. Luo, and T. Jiang (2018). Beam selection for mmwave massive mimo systems under hybrid transceiver architecture. *IEEE Communications Letters 22*(7), 1498–1501.

Rappaport, T. S., S. Sun, R. Mayzus, H. Zhao, Y. Azar, K. Wang, G. N. Wong, J. K. Schulz, M. Samimi, and F. Gutierrez (2013). Millimeter wave mobile communications for 5g cellular: It will work! *IEEE access 1*, 335–349.

Sayeed, A. (2002). Deconstructing multiantenna fading channels. *IEEE Transactions on Signal Processing 50*(10), 2563–2579.

Sayeed, A. and J. Brady (2013). Beamspace mimo for high-dimensional multiuser communication at millimeter-wave frequencies. In *2013 IEEE global communications conference (GLOBECOM)*, pp. 3679–3684. IEEE.

Sayeed, A. M. and T. Sivanadyan (2010). Wireless communication and sensing in multipath environments using multi-antenna transceivers. In *Handbook on Array Processing and Sensor Networks*. Wiley Online Library.

Shafi, M., J. Zhang, H. Tataria, A. F. Molisch, S. Sun, T. S. Rappaport, F. Tufvesson, S. Wu, and K. Kitao (2018). Microwave vs. millimeter-wave propagation channels: Key differences and impact on 5g cellular systems. *IEEE Communications Magazine 56*(12), 14–20.

Xiao, M., S. Mumtaz, Y. Huang, L. Dai, Y. Li, M. Matthaiou, G. K. Karagiannidis, E. Björnson, K. Yang, I. Chih-Lin, et al. (2017). Millimeter wave communications for future mobile networks. *IEEE Journal on Selected Areas in Communications 35*(9), 1909–1935.